Critical mineral pathfinder targeting in the Aravalli basement (northwest India) calibrated against age and tectonically-matched Western Australian analogues using the AuScope EarthBank platform

B. H. Lodhia, P. Agrahari, A. Priyadarshi, B. I. A. McInnes

John de Laeter Centre, Curtin University, Perth, Western Australia

Abstract Critical mineral element fingerprints established in Australian regional geochemistry could accelerate exploration in geologically comparable but less-characterised terranes of north-west India, provided that a defensible basis for comparison can be established. We present a drainage-based method for identifying age and tectonically-matched Australian analogues for north-west Indian stream-sediment geochemistry, for testing whether pathfinder element signatures transfer between them, and for mapping the transferred signatures across the Indian drainage catchments. Sample sets were defined on both continents by drainage containment, tracing each stream-sediment catchment through level-12 hydrological sub-basins and retaining only samples whose upstream catchment lies within a target basement domain. In northwest India these are the Archaean Mangalwar Complex and the Palaeoproterozoic Sandmata Complex of the Aravalli Craton. In Western Australia, they are the coeval Palaeoproterozoic terranes of Western Australia and the Youanmi and Narryer terranes of the Yilgarn Craton. From these sets, we build 20 robust analogue pairs, matched on weathering-robust provenance ratios standardised within each survey and all of which are mutual nearest neighbours at a median separation of less than half a standard deviation. Testing against an independent set of critical mineral pathfinder elements shows that the light rare-earth signature transfers significantly between matched catchments and survives false-discovery-rate control, whereas the heavy rare-earth signature falls just short of that threshold and the hydraulically sorted heavy minerals, such as zircon and titanium oxides, do not transfer. Applying the transferable Australian fingerprint to the Indian samples maps the drainage catchments of the Aravalli basement where the light rare-earth signature is elevated. Hence, Australian critical mineral fingerprints can be carried across to Indian stream-sediment data to map the catchment-scale rare-earth signature, from which exploration hypotheses can be framed and tested.

Keywords: stream-sediment geochemistry; critical minerals; provenance analogues; Aravalli Craton; Yilgarn Craton.

1 Introduction

Regional stream-sediment geochemistry is a primary tool for critical mineral exploration at the catchment scale. Australia has invested in continent-wide, quality-controlled geochemical and heavy-mineral coverage through the National Geochemical Survey of Australia (NGSA) and the Heavy Mineral Map of Australia (HMMA), from which element associations diagnostic of critical mineral hosts have been characterised (de Caritat et al., 2022; de Caritat and Cooper, 2016; Walker et al., 2024). Northwest India is prospective for the same commodities but is less uniformly characterised at the continental scale. If element fingerprints established in Australia could be applied to Indian survey data, exploration targeting in India could be accelerated, but only if a defensible, like-for-like basis for comparison is first established rather than assumed.

Two conditions must hold for such a transfer to be valid. First, the regions compared should be genuinely comparable in age and tectonic setting, so that similar source rocks and mineralising processes can reasonably be expected. Second, the comparison must be made between equivalent sample media and on variables that reflect source-rock character rather than surface processes or inter-survey method differences. Stream sediments integrate all lithologies upstream of a sample site, so a comparison based on bulk chemistry or on bedrock identity risks conflating provenance with weathering, hydraulic sorting and laboratory effects.

This paper develops and applies a method that addresses both conditions. First, we match Western Australian and northwest Indian river catchments that drain age-equivalent cratonic basement, using drainage topology to define the sample sets and weathering-robust provenance ratios to pair them. Second, we test whether pathfinder element signatures transfer between the matched pairs using an independent set of elements. Third, we apply the fingerprints that transfer to score the northwest Indian catchments, which maps the pathfinder element signature across the Aravalli basement.

1.1 Geology of NW India and Western Australia

The Aravalli Craton of northwest India forms the Precambrian basement of Rajasthan and preserves a two-part crustal architecture (Figure 1). An Archaean granite-gneiss basement, the Banded Gneissic Complex, which includes the Mewar and Mangalwar gneisses, is flanked by the reworked Palaeoproterozoic to Mesoproterozoic supracrustal fold belts, the Aravalli and Delhi Supergroups (Fareeduddin and Banerjee, 2020; Ghosh et al., 2022). Within this basement, the granulite-facies Sandmata Complex records late Palaeoproterozoic high-grade metamorphism; Ghosh et al. (2026) date tonalite-trondhjemite-granodiorite (TTG) gneiss protoliths in the Sandmata Complex at approximately 1.82 billion years. The craton has a long metallogenic history and hosts substantial base- and critical-metal mineralisation (Deb, 2014). It lacks, however, the uniform continent-scale geochemical characterisation now available for Australia.

Western Australia exposes cratonic crust of comparable antiquity and architecture (Figure 2). The Yilgarn Craton is a large Archaean granite-greenstone and gneiss province assembled from components of contrasting age and history (Myers, 1995). Its western Narryer and Youanmi terranes preserve Eoarchaean to Mesoarchaean gneiss and granite and record the reworking of older crust (Ivanic et al., 2013; Wyche et al., 2012), and its southwestern margin was overprinted by high-grade Palaeoproterozoic metamorphism (Heseldell et al., 2025; Korhonen et al., 2021). Flanking and postdating the Archaean craton, a set of high-grade Palaeoproterozoic terranes, among them the Halls Creek and Lamboo belts to the north and the Capricorn Orogen and Gascoyne Province to the west, record Palaeoproterozoic orogenesis and high-grade metamorphism across the region. As in the Aravalli Craton, these terranes are well mineralised.

The two regions therefore share the elements required for a provenance analogue. Both preserve an Archaean granite-gneiss basement overprinted by high-grade Palaeoproterozoic belts, and both carry a documented base-metal and critical mineral endowment. The Aravalli Craton hosts world-class base-metal sulphide deposits, notably the Rampura-Agucha, Rajpura-Dariba and Zawar zinc-lead-silver systems, together with copper and tungsten mineralisation (Deb, 2014). The Yilgarn Craton and its bordering Palaeoproterozoic terranes host extensive orogenic gold, including the Katanning deposit (Heseldell et al., 2025), and, as mapped continent-wide by the Heavy Mineral Map of Australia, a widespread distribution of rare-earth and other critical mineral host heavy minerals, including the monazite and xenotime targeted in this study (de Caritat et al., 2022). Ghosh et al. (2026) correlate the approximately 1.82-billion-year Sandmata Complex with the approximately 1.85-billion-year Halls Creek Orogen of northern Australia on age and tectonic grounds, which provides a documented geological basis for one of the two analogue pairings examined here: the Palaeoproterozoic Sandmata Complex against the coeval Palaeoproterozoic terranes of Western Australia. On the same grounds, the Archaean gneissic basement of the Aravalli Craton, represented by the Mangalwar Complex, is matched to the Archaean Youanmi and Narryer terranes of the Yilgarn Craton. Whether this geological correspondence also carries a transferable geochemical signature relevant to critical mineral exploration is the question this paper addresses.

The four basement domains are compared in Table 1 across lithological assemblage, age and crustal evolution, metamorphic grade, granitoid character, sedimentary sources, accessory-mineral assemblage, tectonic setting and known rare-earth mineralisation, with a source given for every entry. The Sandmata Complex and the Western Australian Palaeoproterozoic domain share a convergent Palaeoproterozoic history and granitoid suites of the same age, and both carry a documented rare-earth endowment. Sandmata tonalite-trondhjemite-granodiorite protoliths dated at 1818 ± 7 Ma (Ghosh et al., 2026) are coeval with the 1830–1780 Ma Moorarie Supersuite of the Gascoyne Province (Aitken et al., 2014), and megacrystic potassic granitoids cut both domains (Ghosh et al., 2022; Chivas et al., 2019). The Mangalwar Complex and the Youanmi and Narryer terranes share an Archaean granite-gneiss and greenstone architecture produced by protracted crustal melting and reworking (Ahmad et al., 2018; Ivanic et al., 2012; Myers, 1995).

The pairing is a provenance claim, asserting that catchments in the paired domains erode source rocks of comparable age, composition and accessory-mineral inventory, so that weathering-robust element ratios carried into stream sediment behave in a comparable manner. It does not assert equivalent mineral systems, and the two regions are not claimed to host the same ore deposits, or deposits formed by the same processes or at the same time.

Three differences between the paired domains are not reconciled by this comparison and are stated here so that they are read alongside it. At the matched age the Sandmata Complex reached granulite facies at 12.0–15.0 kbar and 815°C (Ghosh et al., 2022), whereas the coeval Capricorn Orogeny reached upper amphibolite facies only locally and greenschist facies elsewhere (Aitken et al., 2014); the domains are matched on protolith age, lithology and tectonic setting, and not on metamorphic pressure. The Mangalwar Complex is Archaean crust that was pervasively reworked at approximately 1.7 Ga (Ahmad et al., 2018), whereas the Youanmi Terrane cratonised at approximately 2600 Ma and carries no comparable overprint, the Narryer Terrane contributing only 3% of the pooled Archaean catchment area. Finally, Fareeduddin and Banerjee (2020) argue that the term Mangalwar Complex is not tenable under current stratigraphic codes, although it is retained here because it is the name under which the geochemical and isotopic data for this domain are published.

Attribute	Sandmata Complex (India)	Western Australian Palaeoproterozoic	Mangalwar Complex (India)	Youanmi and Narryer terranes
Lithological assemblage	Granulite facies: charno-enderbite, mafic granulite, migmatitic gneiss, metapelite; minor calc-silicate, norite, mafic dykes. Cut by the Anjana, Amet and Bhinai granite batholiths. Tonalite-trondhjemite-granodiorite (TTG) gneiss present [1,2].	Gascoyne Province granite and medium- to high-grade metamorphic rock: Leake Spring Metamorphics (1840–1810 Ma) and Pooranoo Metamorphics (1760–1680 Ma), intruded by successive granite supersuites; Glenburgh Terrane to the south. Overlain by the Edmund and Collier basins. One	Amphibolite facies, heterogeneous: gneiss, metasedimentary pelite, carbonate and quartzite, granitoid, amphibolite. Asan Group bimodal gneiss; Sawadri and Tanwan greenstone sequences [7].	Youanmi Terrane granite-greenstone with separately mapped Yilgarn Craton granite. Narryer Terrane high-grade gneiss after granite; minor granodiorite, tonalite, layered basic intrusions, metasedimentary rock [6,8].

Attribute	Sandmata Complex (India)	Western Australian Palaeoproterozoic	Mangalwar Complex (India)	Youanmi and Narryer terranes
		catchment on the Lamboo Province Western Zone [3,4,6].		
Age and crustal evolution	TTG protolith 1818 ± 7 Ma. Charno-enderbite emplacement 1777 ± 21 to 1641 ± 20 Ma. Exhumed on closure of the Aravalli Basin, approximately 1.8–1.7 Ga [1,2].	Orogenies: Ophthalmian approximately 2200 Ma; Glenburgh 2000–1960 Ma; Capricorn 1830–1780 Ma; Mangaroon approximately 1680–1620 Ma. Intracratonic reactivation: Mutherbukin 1385–1170 Ma; Edmundian 1030–950 Ma. Palaeoproterozoic rocks 68% of pooled catchment area [3,4,18].	Archaean crust reworked in the Palaeoproterozoic. Low-silica gneiss approximately 2.44 Ga, depleted-mantle model age 3.31 Ga; high-silica suite approximately 1.7 Ga, model ages 3.54–2.69 Ga [7].	Youanmi 3131–2700 Ma; mapped Yilgarn granites 3010–2600 Ma; Narryer 4000–2600 Ma. Juvenile input approximately 2980 Ma and 2820–2640 Ma; crustal recycling approximately 2750 and 2620 Ma; cratonised approximately 2630–2600 Ma. Mesoarchaean rocks 93% of pooled catchment area [6,9,18].
Metamorphic grade (age-matched event)	Granulite facies, 1836 ± 17 to 1723 ± 10 Ma. Pelitic granulite 6.5–8.5 kbar, 800–900 °C; mafic granulite above 8.0 kbar, 730–820 °C; peak 12.0–15.0 kbar, 815 °C, clockwise path [1].	Capricorn Orogeny, 1830–1780 Ma: upper amphibolite facies in the Yarlarweelor Gneiss Complex, greenschist facies elsewhere. Orogen comprises low-grade volcano-sedimentary belts, high-grade metamorphic belts and granitoid intrusions [4,5,11].	Amphibolite facies [7].	Youanmi (Murchison Domain) typically greenschist facies, generally low grade. Narryer granulite facies at approximately 2700 Ma [8,9].
Granitoid character	TTG gneiss: moderate to high SiO2 and Al2O3; moderate to low K2O/Na2O; high Sr/Y and Zr/Sm; moderate to low chondrite-normalised La/Yb; pronounced positive Eu anomalies. Zircon saturation approximately 845–690 °C. Source: partial melting of hydrated mafic crust in the garnet stability field. Cut by megacrystic potassic granitoids [1,2].	Dalgaringa 2002–1975 Ma granitic gneiss, supra-subduction geochemistry, continental-margin arc; Bertibubba 1961–1945 Ma; Moorarie 1820–1775 Ma including the Minnie Creek batholith 1808–1786 Ma; Durlacher 1680–1620 Ma megacrystic K-feldspar-phyric monzogranite; Thirty Three 995–940 Ma leucogranite with rare-earth-bearing pegmatite. Moorarie at the Burringurrah type locality: porphyritic biotite monzogranite, rounded K-feldspar phenocrysts to 5 cm [4,5,10,12].	Two potassic, calc-alkaline, peraluminous suites. Low-silica: enriched in K, Sr, Ba, MgO, Cr, Ni; fractionated rare earths (mean chondrite-normalised La/Yb 12.1); small Eu anomaly; Mg number 0.53; akin to Archaean sanukitoids. High-silica: depleted in compatible elements; partial re-melting of older TTG crust [7].	Polelle Group calc-alkaline intermediate to silicic volcanism approximately 2760–2753 Ma with coeval Cullculli and Eelya intrusions sourced over a wide range of crustal depths; post-volcanic granites approximately 2710–2600 Ma, progressive fractionation from an evolving crustal source [9].
Sedimentary sources and cover	Between the Aravalli Supergroup (approximately 2.2–1.7 Ga) and Delhi Supergroup (approximately 1.7–0.7 Ga) metasedimentary sequences [1].	Marginal basins filled with detritus from the Yilgarn Craton, the Gascoyne Complex and an unexposed early Palaeoproterozoic terrane. Upper Wyloo and Capricorn groups 1830–1800 Ma, Ashburton Basin. Edmund Basin 1620–1465 Ma, half grabens covering much of the Gascoyne Province. Pooled catchment area: Edmund 24.3, Collier 9.0, Ashburton 3.7% [3,4,18].	Metasedimentary pelite, carbonate and quartzite within the complex. Banas Dislocation Zone to the north; Banded Gneissic Complex and Aravalli Supergroup to the south [7].	Minimal younger cover; Palaeoproterozoic basins below 3% of pooled catchment area. Narryer quartzite, pelite and banded iron formation deposited 3100–2700 Ma, detrital zircon to 4270 Ma [8,18].
Accessory-mineral assemblage	Apatite, zircon, titanite, calcite; ilmenite to approximately 1.9%. Monazite widely present, used for U-Th-Pb geochronology [1,2].	Measured grain counts, median per site, every phase detected at all ten sites: ilmenite 4458, rutile 1978, zircon 237, apatite 69, monazite 60, xenotime 10, allanite 10, huttonite 11, florencite 10. Monazite and xenotime are established accessory phases in Gascoyne pelitic schists, used there as in situ U-Pb	Apatite, zircon, titanite; biotite the main mafic phase [7].	Measured grain counts, median per site: ilmenite 9138, rutile 2539, zircon 657, monazite 39, xenotime 15, florencite 10, huttonite 4, apatite 3, allanite 2 [18,19].

Attribute	Sandmata Complex (India)	Western Australian Palaeoproterozoic	Mangalwar Complex (India)	Youanmi and Narryer terranes
		geochronometers [10,18].		
Tectonic setting	Late Palaeoproterozoic exhumed high-pressure granulite terrane, western margin of the Aravalli fold belt. Interpreted as an independent terrane with a distinct tectonothermal history rather than reworked basement. TTG geochemistry indicates a mature convergent, subduction-related regime [1,2].	Palaeoproterozoic collisional orogen from suturing of the Pilbara and Yilgarn cratons to form the West Australian Craton; repeatedly reactivated intracratonically through the Meso- and Neoproterozoic. Glenburgh Terrane accreted to the northwestern Yilgarn margin during the Glenburgh Orogeny [3,5].	Reworked granite-greenstone belt, central Aravalli Craton, bounded by the Banas Dislocation Zone. Low-silica suite: slab breakoff and asthenospheric upwelling above a metasomatised mantle wedge [7].	Archaean craton. Mantle plumes at 2.81 and 2.72 Ga drove protracted crustal melting and cratonisation. Narryer and Murchison amalgamated 2.68–2.62 Ga [8,9].
Known rare-earth mineralisation	Allanite-britholite occurrence: migmatite gneiss, Amet Granite (1870 ± 200 Ma) and intrusive syenite and monzonite at Borana, Mad, Rama and Tikar, Rajsamand district. Rare earths interpreted as introduced by fluorine- and phosphorus-rich fluid from the alkaline intrusives [14,15]. Complex assignment differs between sources: see the Mangalwar column.	Yangibana district, Gifford Creek Carbonatite Complex; primary ore mineral monazite, in ankerite-siderite carbonatite, magnetite-biotite dykes and derived ironstones [13]. Rare-earth-bearing pegmatites, Thirty Three Supersuite [5]. Ninety-one rare-earth sites inside six of the ten analogue catchments, including Yangibana, Bald Hill and the Gifford Creek Carbonatite [16,17,18].	The same Borana and Mad occurrence as the Sandmata column. Its authors describe the Amet Granite as a partial melt of Mangalwar Complex migmatite gneiss [15]; Ghosh et al. (2022) instead place the Amet granite among the Sandmata batholiths [1]. Host is Mesoarchaean migmatite gneiss, intrusive is Palaeoproterozoic granite. Reported once, spanning both Indian columns.	Eighteen rare-earth sites inside four of the ten analogue catchments, all undeveloped (Jupiter, Brothers, Iron Duke, Aurora, Juno, Larins Lane, North Stanmore, Cuddingwarra North). No mineralisation style recorded for all but one, so no deposit style is inferred. Mount Weld lies outside every analogue catchment [16,17,18].

Table 1. Comparison of the four basement domains across the attributes required to establish a provenance analogue. Metamorphic grade is quoted for the event age-equivalent to the domain compared and later events are excluded; the Gascoyne Province entries therefore omit the Neoproterozoic Edmundian reworking at greenschist to amphibolite facies at 1030–950 Ma [10], and the Narryer entries omit exhumation at 1800–1600 Ma [8]. The accessory-mineral entries are not equivalent measurements: the Australian columns give grain counts in a heavy-mineral concentrate of a single size fraction, whereas the Indian columns give accessory phases identified petrographically. Rare-earth occurrence counts in the Australian columns are Geological Survey of Western Australia MINEDEX sites falling inside the analogue catchment polygons; the Indian entries are literature records for which no coordinates are published and which could not be tested in the same way. Sources: [1] Ghosh et al. (2022); [2] Ghosh et al. (2026); [3] Cawood and Tyler (2004); [4] Aitken et al. (2014); [5] Johnson et al. (2013); [6] Cutten et al. (2022); [7] Ahmad et al. (2018); [8] Myers (1995); [9] Ivanic et al. (2012); [10] Sheppard et al. (2007); [11] Pirajno (2004); [12] Chivas et al. (2019); [13] Slezak et al. (2021); [14] Guha et al. (2020); [15] Deb (2014); [16] Geological Survey of Western Australia (2026); [17] this study; [18] de Caritat et al. (2023).

2 Data and methods

2.1 Indian and Australian stream sediment geochemistry datasets

The National Geochemical Mapping program (NGCM), conducted by the Geological Survey of India (GSI) is a substantial dataset, comprised of several hundred thousand data points across India. The NGCM program collected samples from 4 unit cells (1 km × 1 km) and combined these to form composite cells (2 km × 2 km). Details of the methodology used to collect samples for the NGCM program are found in Geological Survey of India (2014) and associated literature (e.g., Bagchi et al., 2021). The Australian analogue geochemistry is the National Geochemical Survey of Australia stream-sediment dataset (de Caritat and Cooper, 2016; Walker et al., 2024). The Australian survey analyses a coarse fraction below 2 mm and a fine fraction below 75 µm, each at two sampling depths, and the value used for each site here is the median of those analyses. Indian samples are sieved to −120 mesh, approximately 125 µm, which falls between the two Australian fractions. In the National Geochemical Mapping programme, thorium, scandium, cobalt, niobium, yttrium, zirconium and the major oxides are determined by X-ray fluorescence and the rare earths and hafnium by inductively coupled plasma mass spectrometry, whereas the National Geochemical Survey of Australia determines these elements by inductively coupled plasma mass spectrometry on its total-digestion suite, with the exception of titanium and phosphorus, which are determined by X-ray fluorescence. Lower limits of detection are reported by the Australian survey for every element, at 0.02–0.3 ppm for the trace elements used here and at 30 and 22 ppm for titanium and phosphorus respectively, and values below these limits are flagged with a less-than operator. Such values, and elements not reported at all, are treated as missing rather than replaced by a substitute concentration, and only samples carrying the complete element suite are used in the matching and the scoring.

Drainage topology on both continents uses HydroSHEDS HydroRIVERS and HydroBASINS level-12 sub-basins (Lehner and Grill, 2013). Basement domain boundaries in Western Australia follow the Geological Survey of Western Australia 1:500 000 tectonic-units layer (Cutten et al., 2022).

2.2 The AuScope EarthBank platform

Both the Indian and Australian geochemical datasets used here were standardised to a common data model and ingested into the AuScope EarthBank (EarthBank) platform, an open, cloud-based system for the preservation, dissemination and synthesis of geochemical data (Boone et al., 2022; Nixon et al., 2025). The EarthBank platform combines a geosample registry, structured data repository and integrated analysis tools, and organises analyses under community-agreed database schemas to support Findable, Accessible, Interoperable and Reusable (FAIR) data practice (Wilkinson et al., 2016). EarthBank's major and trace element data framework accommodates the whole-rock and stream-sediment compositions used in this study (Nixon et al., 2025). Standardising the NGCM and the NGSA datasets to this common schema places the two surveys in a single, queryable structure, so that samples, associated metadata and element concentrations can be interrogated and compared on a like-for-like basis, and underpins the kind of integrated, spatially-referenced quantitative analysis of geochemical data applied here.

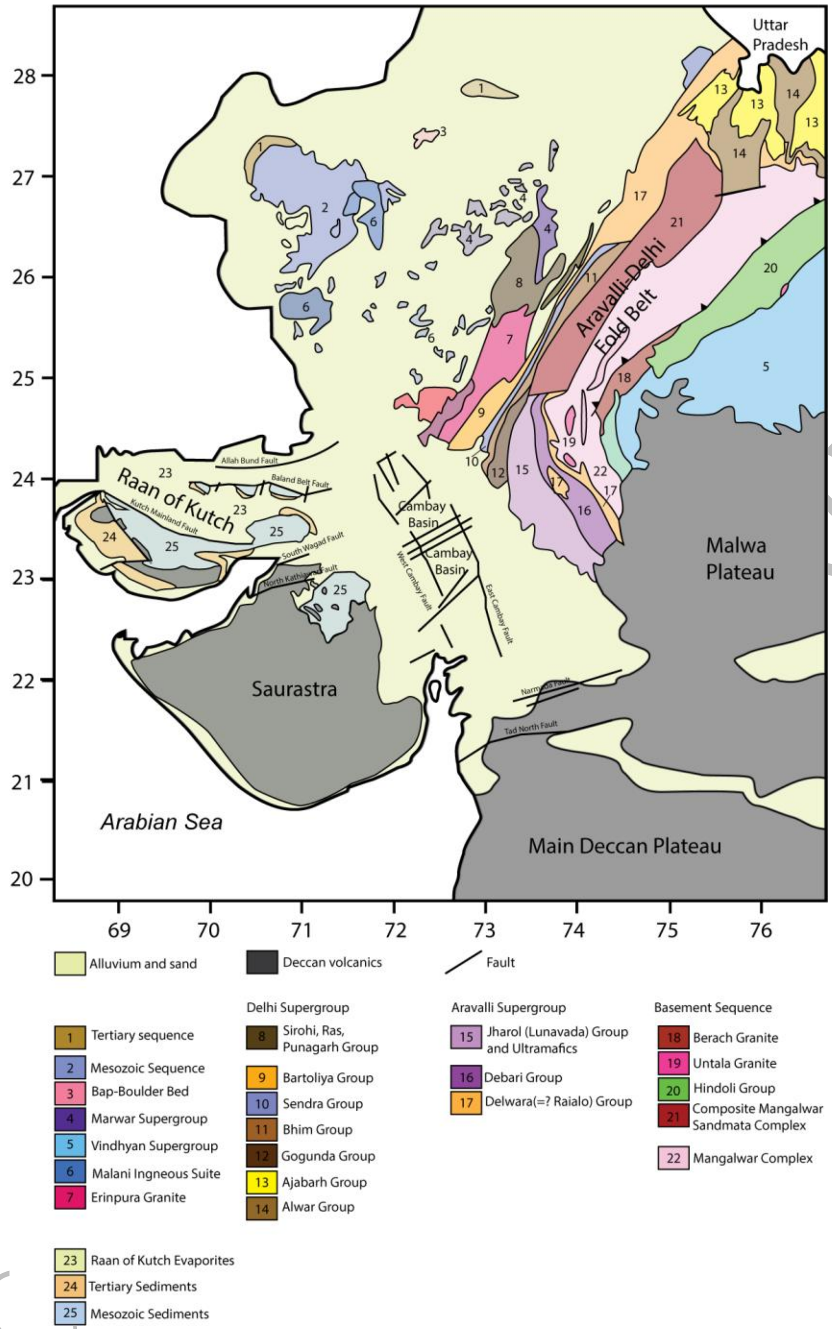

Figure 1. Simplified geological map of north-west India (Rajasthan and Gujarat), compiled for this study. The map shows the lithostratigraphy of the Aravalli Craton, comprising the Banded Gneissic Complex basement (the Mangalwar and composite Mangalwar–Sandmata complexes, and the Berach, Untala and Gingla granites), the Aravalli and Delhi Supergroups and associated granites (units 1–22), together with the Vindhyan and Marwar Supergroups and the Malani Igneous Suite. Also shown are the Mesozoic and Tertiary cover, the Deccan volcanic rocks of the Malwa Plateau and main Deccan Plateau, the Mesozoic and Tertiary sediments and evaporites of Saurashtra and the Rann of Kutch, and the principal bounding faults of the Kutch and Cambay basins. Aravalli Craton lithostratigraphy after Fareeduddin and Banerjee (2020); Deccan and intertrappean beds after Valdiya (2015); Saurashtra Deccan geology after Naushad et al. (2019).

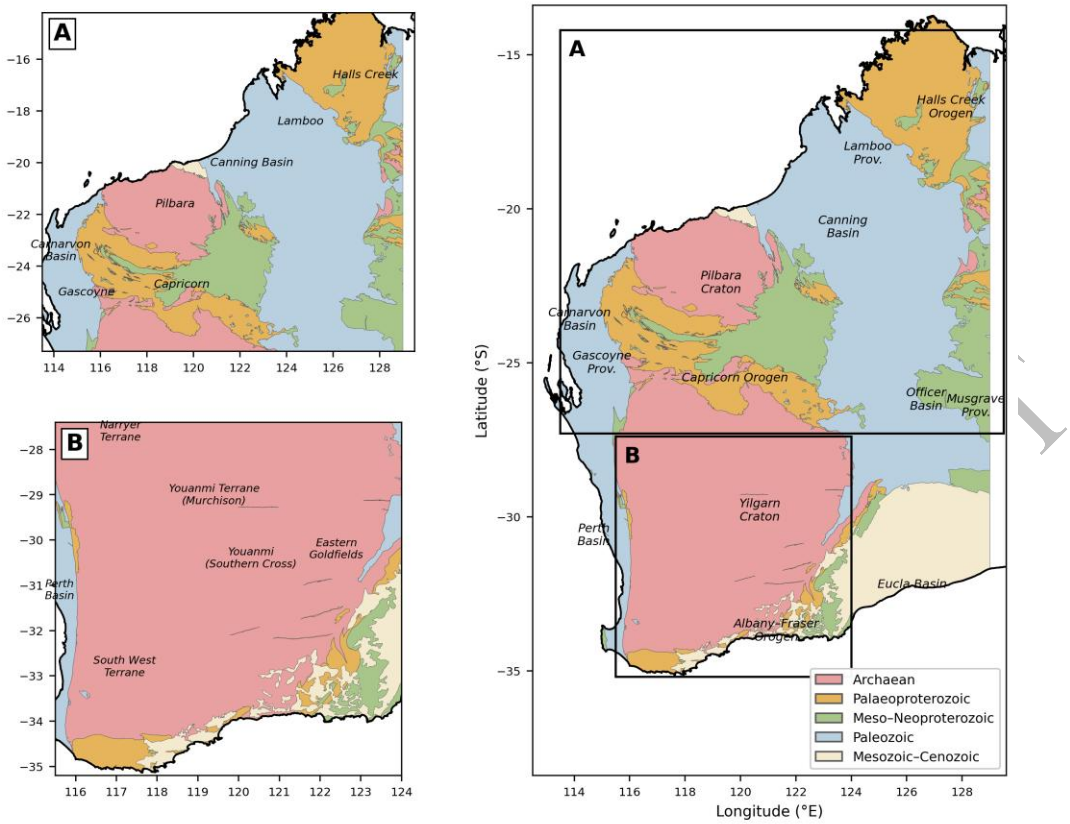

Figure 2. Simplified geology of Western Australia, generalised into five age classes (Archaean, Palaeoproterozoic, Meso–Neoproterozoic, Palaeozoic, and Mesozoic–Cenozoic cover) from the Geological Survey of Western Australia state compilation (Martin et al., 2015). The main panel shows the whole of Western Australia with the principal cratons, orogens, provinces and basins labelled. Boxes A and B mark the areas enlarged in the insets: (A) the Palaeoproterozoic terranes of the north and west, the Gascoyne Province, Capricorn Orogen, Halls Creek Orogen and Lamboo Province, which host the Palaeoproterozoic analogue catchments; and (B) the Yilgarn Craton, showing the Youanmi (Murchison and Southern Cross domains), Narryer, South West and Eastern Goldfields terranes, which host the Archaean analogue catchments.

2.3 Domain definition by drainage containment, analogue matching and within-survey standardisation

Each analogue sample set is defined by drainage containment rather than by a geographic box. The HydroBASINS level-12 sub-basin is the smallest drainage unit and forms the base cell of this scheme; the catchment analysed for a sample is not this single cell but the entire area that drains to the sample site. For every stream-sediment sample point p, the upstream catchment $C(p)$ is assembled by identifying the level-12 sub-basin containing p and then recursively adding every sub-basin that drains into it, following the HydroBASINS next-down topology (Lehner and Grill, 2013); $C(p)$ is therefore the union of many level-12 sub-basins and is typically far larger than any individual sub-basin. The catchment area is the sum of the constituent sub-basin areas, $A\big(C(p)\big) = \sum_{b \in C(p)} A_b$, and the containment fraction is the proportion of that area lying within the target basement domain polygon D,

$$f(p) = \frac{A(C(p) \cap D)}{A\big(C(p)\big)}.$$

A sample is retained when its containment fraction exceeds a threshold. Indian sets use a 50% threshold ($f(p) \geq 0.5$); the larger Australian catchments, which cross terrane boundaries, use a 25% threshold ($f(p) \geq 0.25$). This procedure yields four sets: the Sandmata Complex and Mangalwar Complex catchments in India, and the Western Australian Palaeoproterozoic and Youanmi plus Narryer catchments in Australia. The Australian Palaeoproterozoic pool combines the Halls Creek, Lamboo, Capricorn and Gascoyne terranes, which are coeval with the Sandmata Complex at approximately 1.95 to 1.77 billion years.

Catchments are paired on six provenance-sensitive element ratios (Th/Sc, La/Sc, Th/Co, Eu/Eu*, chondrite-normalised $(\mathrm{La/Yb})_N$, and Nb/Y). These ratios use elements of low aqueous solubility that are carried into clastic sediment with little chemical fractionation, hence the ratios retain the character of the source rock through weathering (McLennan et al., 1993; Taylor and McLennan, 1985). The elements sit largely in accessory minerals: Th in monazite, zircon and allanite; the light rare earths in monazite, allanite and apatite; the heavy rare earths and Y in xenotime, zircon and garnet; and Nb in Ti-oxides. Scandium and cobalt instead follow the ferromagnesian silicates, and europium the feldspar. As several of these hosts are dense accessory phases, the ratios are not wholly free of hydraulic sorting, an effect limited here by standardising each ratio within its own survey and by matching on all six ratios jointly.

The europium anomaly and rare-earth normalisation use the chondritic (CI) values of McDonough and Sun (1995):

$$\mathrm{Eu/Eu^*} = \frac{\mathrm{Eu}_N}{\sqrt{\mathrm{Sm}_N\,\mathrm{Gd}_N}}, \qquad (\mathrm{La/Yb})_N = \frac{\mathrm{La/Yb}}{\mathrm{La}_{CI}/\mathrm{Yb}_{CI}},$$

where subscript N denotes normalisation to the CI values of McDonough and Sun (1995) (La 0.237, Yb 0.170, Sm 0.148, Eu 0.0580, Gd 0.199 ppm).

Because the Australian and Indian surveys use different laboratories, digestions and grain-size fractions, a systematic inter-survey offset is expected; where surveys are merged this is removed by levelling (Grunsky, 2010; Grunsky et al., 2026; Grunsky and de Caritat, 2020). No spatial overlap or shared reference materials exist between the two surveys, so formal levelling is not possible. Each ratio r_k is therefore log-transformed and standardised within its own survey $s \in \{\mathrm{NGSA, NGCM}\}$ to a z-score (Singer and Kouda, 2001):

$$z_k^s = \frac{\ln r_k - \mu_k^s}{\sigma_k^s},$$

where μ_k^s and σ_k^s are the mean and standard deviation of $\ln r_k$ over all drainage-selected catchments of survey s. Matching is thus on relative geochemical character within each survey rather than on absolute concentration. The dissimilarity between Indian catchment i and Australian catchment j is the Euclidean distance in standardised log-ratio space over the six ratios,

$$d(i,j) = \sqrt{\sum_{k=1}^{6} \left(z_{i,k} - z_{j,k}\right)^2}.$$

A pair (i, j) is retained as an analogue only if it is a mutual nearest neighbour, that is $j = \mathrm{argmin}_{j'} d(i, j')$ and simultaneously $i = \mathrm{argmin}_{i'} d(i', j)$; the robust set comprises the mutual nearest neighbours of smallest d.

2.4 Fingerprint transfer and catchment scoring

Each analogue links one Indian catchment to a geochemically and geologically equivalent Australian catchment. Because the Australian coverage is characterised for the element associations that host critical minerals, a fingerprint measured on the Australian side can be evaluated on the matched Indian side. We define a set of critical mineral pathfinder fingerprints, each a small group of elements diagnostic of a heavy-mineral host (Table 2). These pathfinder elements are not used directly in the matching, though some share their accessory-mineral hosts, monazite and xenotime, with the rare-earth ratios used to pair the catchments. The transfer test is therefore best read as a check that provenance-matched catchments share their critical mineral fingerprints, rather than as a test fully independent of the matching.

For each catchment a within-survey standardised log-abundance is computed for every pathfinder element e,

$$g_e^s = \frac{\ln a_e - \mu_e^s}{\sigma_e^s},$$

where a_e is the element concentration and μ_e^s, σ_e^s its log-mean and log-standard-deviation within survey s; a per-mineral fingerprint score is the mean of g_e^s over that mineral's elements. Whether a fingerprint transfers is tested by the Spearman rank correlation between the paired Indian and Australian per-mineral scores over the twenty pairs. Its significance is assessed by a hundred-thousand-permutation test that randomly re-pairs the Indian and Australian catchments to build the null distribution of the correlation. Because five fingerprints are tested at the same time, the chance that at least one returns a spuriously significant correlation is inflated; to control this, the per-fingerprint probabilities are adjusted to false-discovery-rate q-values by the Benjamini and Hochberg (1995) procedure, which bounds the expected proportion of false positives among the fingerprints declared to transfer. A fingerprint is accepted as transferable only where its corrected q-value falls below 0.05, and on this criterion the light rare-earth fingerprint passes whereas the heavy rare-earth fingerprint does not, falling just short at 0.059 (Table 2). Each transferable fingerprint is then applied to every drainage-selected Indian sample, whose per-mineral score (the mean of g_e^s over that mineral's elements, Equation 5) is the per-catchment pathfinder value mapped in Section 3.3.

Fingerprint	Fingerprint elements	Spearman ρ	p	q	Transfers
Light rare earths, monazite-associated	Ce, Nd, Pr	0.70	0.001	0.004	Yes
Heavy rare earths, host not resolved	Dy	0.51	0.024	0.059	Borderline
Zirconium and hafnium, zircon-associated	Zr, Hf	0.31	0.18	0.30	No
Titanium, titanium-oxide-associated	Ti	−0.24	0.31	0.38	No
Phosphorus, apatite-associated	P	0.13	0.58	0.58	No

Table 2. Critical mineral pathfinder fingerprints evaluated on the matched analogue pairs, and their transfer between the Indian and Australian catchments. The fingerprint elements are not used in the matching. Transfer is the Spearman rank correlation of the paired per-

mineral scores over the twenty pairs ($n = 20$), with permutation significance p and the Benjamini–Hochberg false-discovery-rate value q computed across the five fingerprints. Only the light rare-earth fingerprint reaches $q < 0.05$ and is carried forward to the catchment mapping, whereas the heavy rare-earth fingerprint is not counted as reliably transferable and is shown in Figure 5b for comparison. Table 7 reports the stability of these correlations under resampling. Each fingerprint is named for the element association it measures and for the phase with which that association is most commonly identified; the names are not mineral identifications, and the associations are tested against measured grain counts in Table 9.

2.5 Limitations

Several limitations should be noted. The Australian sample counts are small because National Geochemical Survey of Australia catchments are large and cross terrane boundaries, so the robust pair set is the closest-matching subset rather than an exhaustive sample. The domain polygons are digitised from generalised maps and carry positional uncertainty of the order of ten kilometres. The two surveys also differ in sample support and preparation: the Indian samples are 2×2 km composites sieved to a finer fraction (minus 120 mesh) than the National Geochemical Survey of Australia fractions (Bagchi et al., 2021), so the within-survey standardisation additionally absorbs this grain-size and support difference, which is a further reason the sorting-controlled heavy minerals (zircon, titanium oxides) are not expected to transfer. Grain size is not incidental, since rebuilding the matching and the transfer from the coarse Australian fraction alone selects a different set of pairs and returns no transfer, whereas the fine fraction, which is closer to the Indian sieve size, retains it. Standardisation is applied within each survey, so the catchment scores mapped in Section 3.3 rank Indian catchments against one another rather than estimating absolute abundance, and an Indian catchment richer in rare earths than its Australian analogue does not appear richer once standardised. The paired samples do differ in absolute terms, the Indian samples carrying approximately 2.8 times the light rare-earth concentration of their matched Australian analogues, but that ratio cannot be read as a geological enrichment, since it also carries the difference in size fraction and digestion between the two surveys, and since the two landscapes differ in weathering history (Chivas et al., 2019). The transfer result does not depend on this choice, because a rank correlation is unchanged by any transformation applied within a survey, and recomputing it without standardisation, with pooled standardisation across both surveys, with robust median and median-absolute-deviation scaling, and on within-survey percentile ranks changes no correlation by more than 0.001. The analogue currently rests on the Palaeoproterozoic and Archaean pairs examined here, and extension to further terranes would strengthen the generality of the conclusions. The two regions also differ in their post-orogenic weathering histories, the Australian catchments draining a deeply weathered residual surface on which kaolinitic weathering of the Moorarie Supersuite at Burringurrah is dated to 200–100 Ma and continues into the Neogene, with a long-term denudation rate of approximately 11 m Ma^{-1} on a low-relief land surface capped by a hardened weathering crust (Chivas et al., 2019). No equivalent constraint on the weathering and denudation history of the Aravalli basement is compiled here, so the comparison rests on ratios chosen to be robust to weathering rather than on an assumption that the two landscapes have weathered alike. The precision of the published National Geochemical Mapping coordinates also varies, many being recorded in degrees, minutes and seconds and precise to metres, whereas 18% of the Rajasthan coordinates are stated to two decimal places or fewer, which locates a sample to approximately a kilometre or worse. Each sample is assigned to the sub-basin containing it and its catchment traced upstream from there, so imprecision at that level propagates into the catchment assignment, and its effect on the retained pairs has not been quantified here.

2.6 Code and data availability

The complete analysis is implemented in a code repository, archived at https://doi.org/10.5281/zenodo.22269835, which holds the code behind every result reported here: the drainage containment defining the four sample sets, the analogue matching, the fingerprint transfer, the catchment scoring, the catchment geology, and the sensitivity and validation tests. A schematic of the workflow is included, with a key naming the script that implements each step, and a self-test reproduces the twenty analogue pairs and the transfer correlations before any other script is run. References for source datasets used in this study are provided in the repository.

3 Results

3.1 Robust analogue pairs

Twenty robust analogue pairs were retained, ten in the Palaeoproterozoic domain and ten in the Archaean domain (Figure 3). All are mutual nearest neighbours, and the standardised match distances are small, ranging from 0.25 to 0.66 standard deviations with a median of 0.42, so paired catchments sit within about half a standard deviation of each other in the six-ratio provenance space. Nine of the ten Sandmata analogue catchments drain the Capricorn Orogen, which supplies 73–93% of each catchment area and comprises the Gascoyne Province basement of the Burringurrah Domain and Glenburgh Terrane together with the overlying Edmund and Collier basins, whereas the tenth drains the Halls Creek Orogen, where the Western Zone of the Lamboo Province supplies 55% of the catchment, and Palaeoproterozoic rocks account for 68% of the pooled catchment area of this set. The Mangalwar analogues drain the Yilgarn Craton, where the Youanmi Terrane and the mapped Yilgarn Craton granites together supply 93% of the catchment area and the Narryer Terrane 3%, and Mesoarchaean rocks account for 93% of the pooled area (Table 3). The same measurement places two qualifications on the independence of this set: Palaeoproterozoic pairs 1 and 4 draw on a single catchment, sample sites 2007190003 and 2007190213 lying approximately 150 m apart and sharing an identical 3643 km² catchment, so the set comprises nineteen independent catchments rather than twenty; and Palaeoproterozoic pairs 5, 6 and 7 lie on the same drainage system, so their catchments are nested. Comparing the pairs element by element (Figure 4) shows that the weathering-immobile elements sit on a consistent trend between the two surveys, offset from the one-to-one line by a near-constant factor, while the weathering-mobile elements scatter more widely. The two averaged panels of Figure 4 show this offset directly: the light rare earths are enriched in the Indian samples by a median factor of about 2.8 relative to the matched Australian samples, and thorium and zirconium are also somewhat higher, while the major elements plot close to the one-to-one line. Because the offset is close to constant from pair to pair, it is taken out by the within-survey standardisation used for matching and does not affect the pairing. It is the consistency of the immobile elements, not their absolute agreement, that records the shared provenance; the scatter of the mobile elements is consistent with the two drainage systems differing in weathering and hydraulic sorting.

3.2 Which fingerprints transfer

Tested on the independent pathfinder elements, only the light rare-earth signature transfers significantly between matched catchments and survives false-discovery-rate correction (Table 2). The light rare-earth fingerprint gives a Spearman correlation of 0.70 at a corrected q-value of 0.004, and its individual elements give 0.66 for cerium, 0.68 for neodymium and 0.74 for praseodymium, whereas the heavy rare-earth fingerprint, based on dysprosium, gives 0.51 at a corrected q-value of 0.059 and does not clear the 0.05 threshold. Zircon, titanium oxides and apatite do not transfer significantly. The analogue therefore carries the signature of the rare-earth-bearing critical mineral hosts specifically, whereas the abundances of dense, mechanically robust heavy minerals such as zircon and titanium oxides, which are governed strongly by local hydraulic sorting and by the differing grain-size fractions of the two surveys, do not transfer. Stability of these correlations to the number of pairs was tested by refitting with each pair dropped in turn and by bootstrap resampling, from which confidence intervals were also obtained (Table 7). The light rare-earth correlation is stable, holding at 0.649–0.753 across the leave-one-out refits and clearing the threshold in all twenty, whereas the heavy rare-earth correlation clears it in only nine refits of twenty and carries a bootstrap interval of 0.030–0.796. Whether the matching procedure itself generates these correlations was tested by repeating the transfer under alternative matching algorithms, varied numbers of retained pairs and changed distance thresholds, and against a control population of analogue pairs drawn at random from the same domain pools (Table 8). Every matching variant returns the light rare-earth correlation, which sits at the 99.9th percentile of the random control, and no other fingerprint reaches the 95th. Varying the containment thresholds that define the two catchment sets leaves the Indian side intact at 0.663–0.773 across thresholds of 40–75%, and reduces the Australian side to 0.513 at 40% only where the higher threshold empties the analogue pool, a reduction reproduced by cutting that pool at random to the same size at unchanged containment. The Australian catchments are also much larger than the Indian ones and their fingerprint scores correlate with catchment area, so the transfer was recomputed with the catchment areas of both sides regressed out of the paired scores, and the light rare-earth correlation falls from 0.70 to 0.63 while still clearing the corrected threshold. The mineral associations these fingerprints imply were then tested against measured mineralogy, using the automated grain counts reported by the Heavy Mineral Map of Australia, which are made on the National Geochemical Survey of Australia samples themselves, so that each fingerprint score can be compared with the measured abundance of its candidate host at the same site with no spatial matching involved. Over the drainage-selected Australian pool the light rare-earth fingerprint predicts measured monazite grain counts with a Spearman correlation of 0.581, and 0.551 over the analogue pairs, so that association is supported by measurement rather than assumed. It is not exclusive: the same elements track measured allanite at 0.455, and the light rare-earth occurrence documented in the Indian basement is an allanite-britholite occurrence. The heavy rare-earth fingerprint predicts measured xenotime under no combination of heavy rare-earth elements tested, including yttrium alone, yttrium with dysprosium and the full heavy rare-earth suite, and every combination returns a negative correlation over the analogue pairs. Zirconium with hafnium, titanium and phosphorus are likewise unsupported against their candidate hosts, and the full comparison is given in Table 9.

3.3 Catchment pathfinder scores in the Aravalli basement

Applying the transferable light rare-earth fingerprint to every drainage-selected Indian sample, with the heavy rare-earth fingerprint shown alongside for comparison, scores the Aravalli catchments for their rare-earth element signature (Figure 5). The scores vary systematically across the basement, and the highest-scoring catchments, the top decile within each domain (ringed in Figure 5), identify where the rare-earth element signature is most strongly expressed in the Indian stream sediments. An elevated score records the rare-earth content of the material a catchment drains, and that content may reflect the ordinary accessory-mineral budget of the basement lithologies eroded rather than any mineralisation, so the ranking locates provenance and not fertility. The light rare-earth score derives from a fingerprint demonstrated to transfer from the Australian analogues rather than from raw abundance alone, and the highlighted catchments are therefore put forward as catchment-scale exploration hypotheses for rare-earth-bearing critical minerals within the Aravalli basement, and not as demonstrated occurrences.

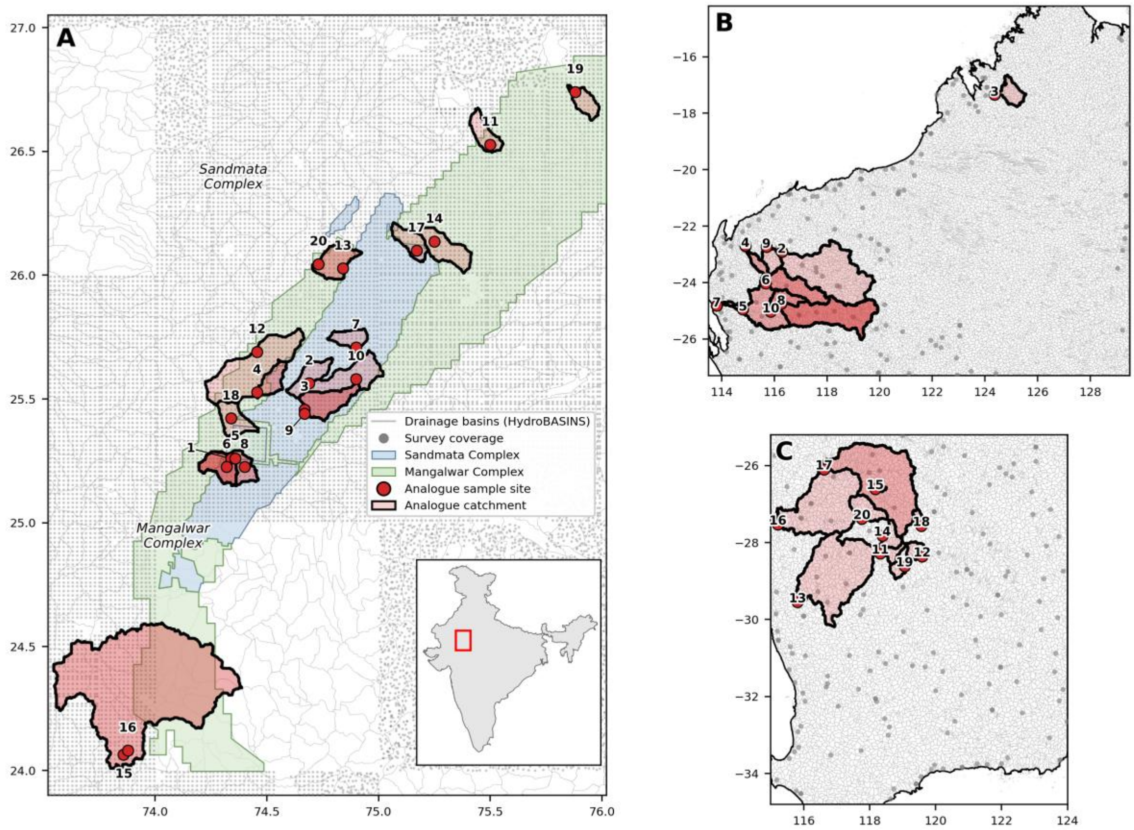

Figure 3. Drainage-defined analogue sample sets and the twenty analogue pairs. (a) North-west India, showing the Archaean Mangalwar Complex and Palaeoproterozoic Sandmata Complex basement domains (shaded), the full National Geochemical Mapping (NGCM) stream-sediment coverage (grey points), and the twenty analogue sample sites (red, numbered 1–20). (b) North-west Australia and (c) the Yilgarn Craton, showing the National Geochemical Survey of Australia (NGSA) coverage (grey points) and the matched analogue sites, the ten Palaeoproterozoic pairs (1–10) in (b) and the ten Archaean pairs (11–20) in (c). In every panel the thick black outlines are the aggregated upstream catchments of the analogue samples, while the faint grey mesh is the individual HydroBASINS level-12 sub-basins from which those catchments are assembled. Drainage from HydroSHEDS HydroBASINS (Lehner and Grill, 2013); Western Australian basement domains from the Geological Survey of Western Australia 1:500 000 tectonic units (Cutten et al., 2022); stream-sediment datasets from the National Geochemical Survey of Australia (de Caritat and Cooper, 2016) and the National Geochemical Mapping programme (Bagchi et al., 2021; Geological Survey of India, 2014); Indian basement domains after Ghosh et al. (2026).

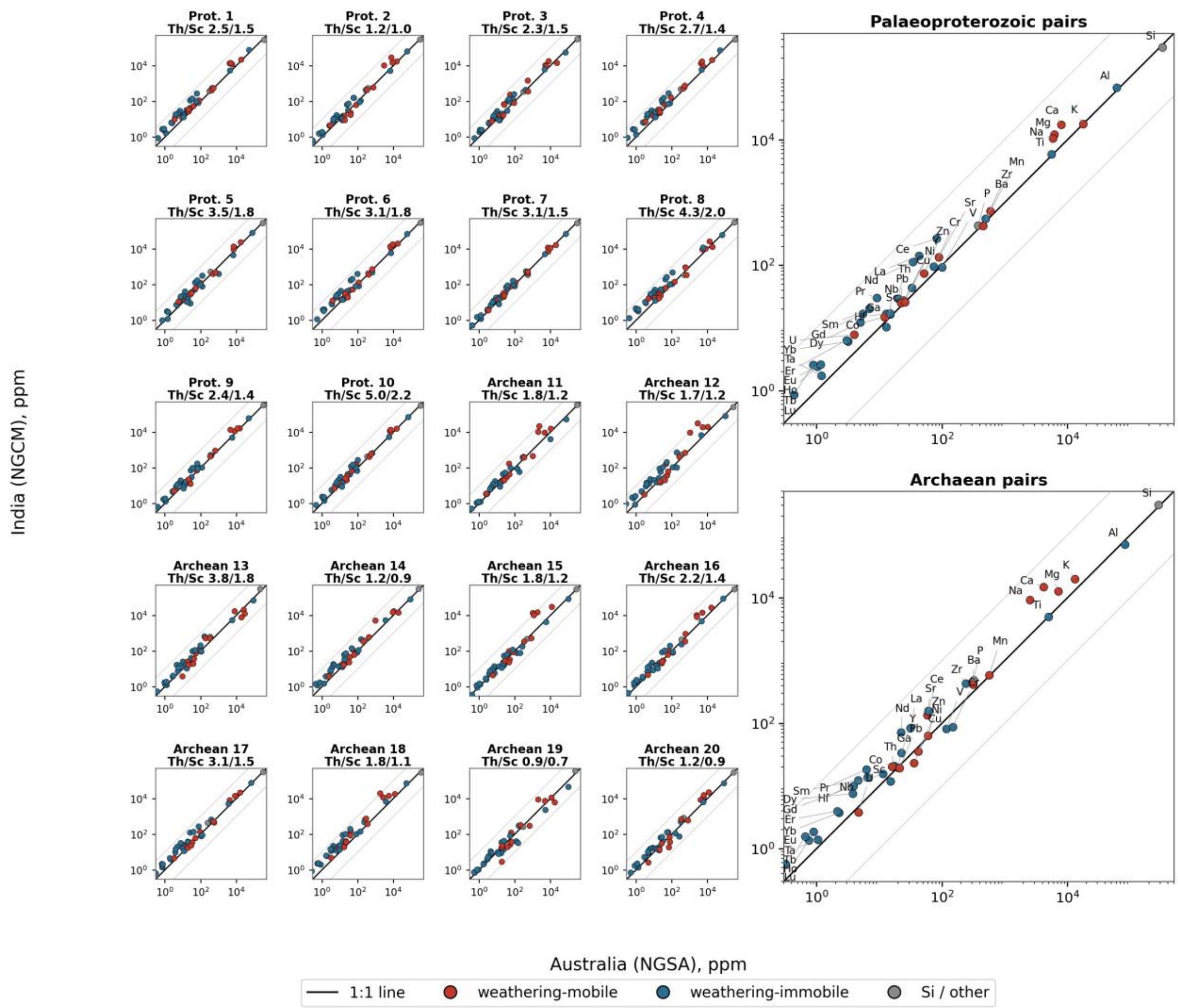

Figure 4. Element-by-element comparison of the twenty robust analogue pairs. Each panel plots, for one analogue pair, the concentration of every element measured by both surveys in the Australian catchment sample (National Geochemical Survey of Australia, NGSA; horizontal axis) against the matched Indian catchment sample (National Geochemical Mapping, NGCM; vertical axis), both in parts per million on logarithmic axes. Australian values are the median of the analyses at that NGSA site. The solid line is the one-to-one relationship and the faint diagonal lines mark factor-of-ten departures from it. Points are coloured by weathering behaviour: weathering-immobile elements (blue), weathering-mobile elements (red), and silicon and other elements (grey). Small panels are ordered by domain, the ten Palaeoproterozoic (Sandmata) pairs labelled Prot. 1 to 10 and the ten Archaean (Mangalwar) pairs labelled Archean 11 to 20, with the numbering matching that of Figure 3; each panel header also gives the Th/Sc ratio of the Indian and Australian sample, in that order. Large right panels: summary of geometric mean of elements across the ten Palaeoproterozoic pairs (upper panel) or the ten Archaean pairs (lower panel), with the elements labelled. In both averaged panels the weathering-immobile light rare earths and thorium plot above the one-to-one line, showing that these elements are enriched in the Indian samples relative to the matched Australian samples, while the major elements plot close to the line. This offset is close to constant from pair to pair and is removed by the within-survey standardisation used for matching; the immobile elements track a consistent proportional relationship between the surveys, consistent with the paired catchments sharing

provenance, while the weathering-mobile elements scatter as expected under differing weathering and hydraulic sorting.

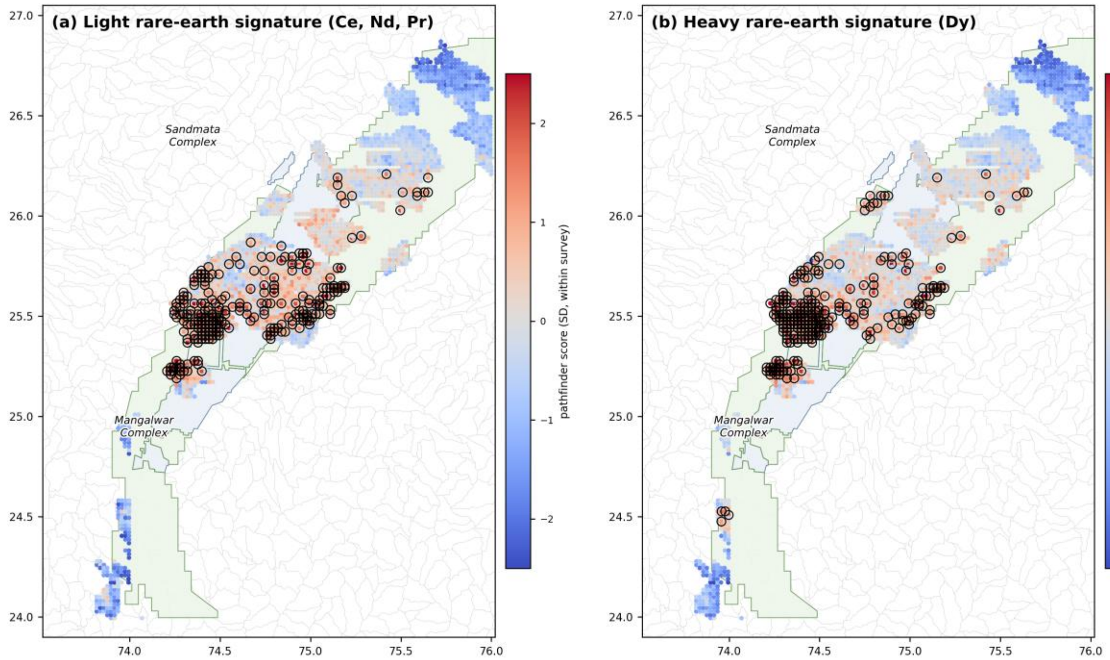

Figure 5. Critical mineral pathfinder scores over the north-west Indian drainage-defined stream-sediment samples, for the two rare-earth fingerprints evaluated on the Australian analogues: (a) the light rare-earth signature (Ce, Nd, Pr), which transfers between the matched catchments, and (b) the heavy rare-earth signature (Dy), which falls just short of the false-discovery-rate threshold and is included for comparison. Each point is a drainage-selected National Geochemical Mapping sample, coloured by its within-survey standardised fingerprint score (Equation 5); warm colours are elevated scores. Black rings mark the top decile within each domain. The shaded areas are the Sandmata (blue) and Mangalwar (green) basement domains and the faint grey mesh is the HydroBASINS level-12 drainage network. Elevated scores in (a) identify the drainage catchments whose provenance carries the transferable light rare-earth fingerprint, whereas the scores in (b) are computed on the same basis but are not carried forward for the reason given above.

4 Discussion

Section 1.1 states that the pairing is a provenance claim and not a claim of equivalent mineral systems, and the levels of claim that follow from it are worth separating because the evidence for each is different. At the first level, a geological analogue requires two domains to share age, lithology, metamorphic history and tectonic setting, and Table 1 sets out that comparison. At the second level, a provenance analogue additionally requires that catchments in those domains erode source material of similar character, which the twenty pairs establish, all being mutual nearest neighbours at a median separation of 0.42 standard deviations in the six-ratio space. Whether the two surveys record that shared provenance consistently defines the third level, and the element-by-element comparison establishes it, the weathering-immobile elements following a near-constant proportional relationship between the surveys (Figure 4). The fourth level, a transferable pathfinder response, is reached where a fingerprint measured in one survey predicts the same fingerprint in the matched catchment of the other, which holds for the light rare-earth signature and fails for zircon, the titanium oxides and apatite (Table 2). Only at the fifth level does the analogue become an exploration hypothesis, under which catchments carrying an elevated transferred signature are held more likely to contain critical mineral occurrences.

The results presented here reach the fourth level, whereas the fifth is proposed and not tested by this work, since no Indian occurrence is used to validate the scored catchments and validation would require follow-up sampling, heavy-mineral separation and dating in the highest-scoring catchments. Indirect support comes from the Australian end of the analogue, set out below, which is evidence that the fingerprint tracks rare-earth endowment where endowment is already known and not evidence that it does so in the Aravalli basement.

The results presented in this study give a practical basis for carrying Australian critical mineral fingerprints across to Indian stream-sediment data. The comparison is made between matched catchment pairs rather than between the whole populations, where inter-survey and weathering differences are likely to dominate. Standardising each provenance ratio within its own survey removes the systematic offset between the two datasets. Pathfinder elements are not used directly in analogue matching. Since the rare-earth pathfinder elements share their mineral hosts with some of the matching ratios, we interpret the transfer as corroborating the analogue rather than as independent proof of it. Full independence at the level of mineral hosts is not achievable, since a matcher able to discriminate rare-earth provenance must use elements that reside in rare-earth-bearing accessory minerals, and relevance to the pathfinder is therefore mutually exclusive with independence from its host. Rebuilding the matching from ratios whose elements occur in none of the targeted minerals confirms this, in that those matchers are of comparable quality but pair catchments on unrelated properties, and no fingerprint transfers between them.

Whether the pattern of mineral fingerprint scores transfer between catchments across NW India and Western Australia is an open question. Whilst zircon and Ti-oxides (e.g. rutile and ilmenite) are both dense ($3.95 - 4.73$ and $4.23 - 4.8$ gcm^{-3}, respectively) and weathering-resistant, they are sensitive to hydraulic sorting and the grain size fraction analysed by surveys. Hence, both zircon and Ti-oxides can vary between catchments despite similar bedrock geology. Our results indicate that these signatures do not transfer between India and Australia. However, such reasoning does not explain why other hydraulically sorted minerals of similar or greater density, such as monazite, give mineral fingerprint scores that do transfer across Indian and Australian analogues. Critical elements such as zirconium, hafnium and titanium partition into specific mineral phases. These are zircon exclusively for Zr and Hf, and mostly rutile and ilmenite for Ti. A catchment's score for these elements is a measure of how much of that one heavy mineral reached the sample point, and is controlled by sorting and grain size accordingly. This cannot be true for rare-earth elements which partition into many mineral phases, such as cerium, neodymium, praseodymium and dysprosium, which are carried by several mineral hosts and by the bulk chemistry of the sediment. Hence, their scores reflect the overall rare-earth character of everything draining the catchment rather than the abundance of one grain type. A signature averaged over many mineral phases is more reproducible between surveys than one carried by a single phase, which accounts for the transfer of the light rare-earth fingerprint and the failure of the single-mineral signatures of zircon and the titanium oxides. This distinction is reinforced by apatite. Phosphorus is concentrated in a single host, apatite, and its fingerprint also fails to transfer (Table 2), yet apatite is not a dense heavy mineral (~ 3.2 gcm^{-3}). Density would predict apatite to behave differently from zircon, whereas it behaves the same, which is what the single-phase argument predicts.

For a relatively under-explored region such as NW India, the results presented in this study provide a means to narrow the initial search for potential critical mineral exploration. Catchment pathfinder scores reflect material deposited from their upstream drainage areas, hence those with high scores highlight regions for further investigation. Such follow-up work may include detailed sampling, heavy-mineral separation, dating and eventually drilling. Each high-scoring catchment identifies a drainage system whose stream sediments carry an elevated rare-earth element signature inherited from an upstream source, and the value of the map lies in directing the next, more detailed, stage of work. For example, the ranked catchments are natural targets for provenance studies: heavy-mineral concentrates separated from the stream sediments can be interrogated grain by grain, and single-grain U–Th–Pb geochronology of the rare-earth phosphates monazite and xenotime can date the mineralising or crystallising event and distinguish magmatic, metamorphic and hydrothermal origins, pointing back towards the bedrock source. Combined with the drainage topology already used to define each catchment, this allows a broad catchment-scale anomaly to be narrowed progressively towards a located occurrence and its mineralising system. The analogue-based scoring therefore concentrates conventional, higher-cost exploration effort, including sampling, dating and follow-up mapping, on the parts of the Aravalli basement where the transferred rare-earth fingerprint is most strongly expressed, and whether those catchments are also the most fertile is the hypothesis that such follow-up would test.

The light rare-earth signature supported by the Heavy Mineral Map of Australia grain counts is carried by the mineral that constitutes the ore at the principal rare-earth deposit of the analogue region. The Yangibana district lies within the Gascoyne Province, drained by nine of the ten Palaeoproterozoic analogue catchments, and its primary ore mineral is monazite, hosted in ankerite-siderite carbonatite, magnetite-biotite dykes and derived ironstones of the Gifford Creek Carbonatite Complex (Slezak et al., 2021). Rare-earth occurrences across the Capricorn Orogen are localised on lithospheric-scale structures, Gifford Creek lying on the Lyons River, Minnie Creek and Minga Bar fault system (Johnson et al., 2013). Testing the sites of the MINEDEX database (Geological Survey of Western Australia, 2026) against the catchment polygons places Yangibana, Bald Hill and the Gifford Creek Carbonatite inside three of the ten Palaeoproterozoic analogue catchments, so the correspondence holds at the scale of a mineral deposit and not only at that of individual grains.

Because the analogue pairs are matched on the properties of the source rocks, the relevant comparison is with the granitic basement that hosts the Gifford Creek Carbonatite Complex, emplaced at approximately 1.8 Ga (Pearson and Taylor, 1996), which is the age of the Sandmata Complex tonalite-trondhjemite-granodiorite protoliths at 1818 ± 7 Ma (Ghosh et al., 2026), whereas the carbonatitic magmatism that formed the ore is younger, at approximately 1.25 Ga.

A comparable light rare-earth occurrence is documented in the Indian basement, where allanite and britholite occur in migmatite gneiss, in the Amet Granite dated at 1870 ± 200 Ma, and in intrusive syenite and monzonite at Borana, Mad, Rama and Tikar in Rajsamand district, the rare earths being interpreted as introduced by fluorine- and phosphorus-rich fluid derived from the alkaline intrusives (Guha et al., 2020). Guha et al. (2020) assign the host migmatite gneisses to the Mangalwar Complex, whereas Ghosh et al. (2022) place the Amet granite among the batholiths of the Sandmata Complex, so the occurrence is reported here as spanning both Indian domains. Its carrier mineral is allanite, which the mineralogical validation also identifies as a carrier of the light rare-earth signature alongside monazite, although no published coordinates are available for this occurrence, so it could not be tested against the Indian catchment polygons in the way the Australian occurrences were.

Monazite and xenotime are both established accessory phases in pelitic schists of the Gascoyne Province, where they are used as in situ U-Pb geochronometers (Sheppard et al., 2007), so the heavy rare-earth signature was a reasonable expectation on mineralogical grounds, and its failure to correlate with measured xenotime abundance is a statement about detectability in the available grain counts rather than about the absence of the mineral.

4.1 Application within the India–Australia critical minerals partnership

The approach demonstrated here is timely in the current policy context. On 9 July 2026, the governments of Australia and India announced a refreshed Memorandum of Understanding between Geoscience Australia and the Geological Survey of India, described as providing "a framework for science exchanges to support resource mapping and mineral exploration" (Albanese et al., 2026). The Australian Minister for Resources noted that the agreement between the two geological organisations would help to uncover potential new deposits of critical minerals in support of the two countries' economic partnership. The method presented in this paper exemplifies the science exchange that such an agreement is intended to enable: it takes characterised Australian survey data and applies it, through a defensible provenance analogue, to guide critical mineral targeting in Indian survey data.

Realising this at scale depends on the two surveys' data being interoperable. The Australian datasets used here are curated in the AuScope EarthBank platform, Australia's national geoscience data infrastructure, which standardises geochemical and geochronological data to community-agreed schemas and makes them queryable alongside their metadata. Ingesting Indian National Geochemical Mapping data into the same infrastructure, as was done for the samples analysed here, places the two national datasets in a single structure in which analogue matching, fingerprint transfer and catchment scoring can be carried out directly and reproducibly. Given the political commitment now in place, there is clear mutual benefit in the Geological Survey of India developing a data-infrastructure collaboration with EarthBank, so that the bilateral exchange of geoscience data envisaged by the Memorandum of Understanding can be operationalised on a shared, standards-based platform rather than through bespoke, one-off transfers.

Beyond acting as a shared repository, the platform's synthesis capability is what makes it valuable for exploration. AuScope EarthBank is built to compare and contrast geoscience datasets of different types, including geochemical, geochronological and thermochronological data, within a single relational data model (Boone et al., 2022; Nixon et al., 2025), and to place samples in their deep-time context through integrated plate-tectonic reconstruction (Boone et al., 2023). For critical mineral exploration this extends the analogue principle used here. Provenance matching need not rest on stream-sediment geochemistry alone, since age and isotopic data held under the same schema allow candidate analogue catchments to be corroborated on independent evidence before their fingerprints are transferred. Building the bilateral geoscience exchange on a platform with these capabilities would therefore let the method demonstrated here scale from stream-sediment analogues to a multi-dataset framework for joint critical mineral targeting. The geochemistry data model underlying the platform is itself under active development, with work in progress to record the analytical method behind each result, to carry a fuller description of the material sampled and the manner of its collection, and to preserve analytical results reported qualitatively rather than as a concentration. That development bears directly on comparisons of the kind made here, drawn from two continent-scale surveys that differ in size fraction, digestion and instrument, because the harmonisation carried out manually in Section 2.1 is the step such a data model is intended to make explicit and repeatable. Combined with the reconstruction capability described above, which places a sample in the palaeogeographic setting of its source rather than at its present-day coordinates, this would allow analogue catchments on now-separated cratons to be identified and compared on a consistent analytical basis.

5 Conclusions

A drainage-based method identifies age- and tectonically-matched Australian analogues for north-west Indian stream-sediment geochemistry, tests whether pathfinder element signatures transfer between them, and maps the transferred signatures across the Indian catchments. Sample sets defined by drainage containment on both continents yield twenty robust analogue pairs, all mutual nearest neighbours matched on weathering-robust provenance ratios standardised within each survey. Tested on an independent set of pathfinder elements, the light rare-earth signature transfers significantly between matched catchments, whereas the heavy rare-earth signature falls just short of the false-discovery-rate threshold and the hydraulically sorted heavy minerals do not transfer. Applying the transferable fingerprint to the Indian samples maps the Aravalli catchments where the light rare-earth signature is elevated. Together these results provide a transferable framework for applying Australian critical mineral element fingerprints to Indian survey data, most reliably for the rare-earth-bearing critical minerals.

Declaration of generative AI and AI-assisted technologies in the manuscript preparation process

During the preparation of this work the authors used Claude (Anthropic) to help refine the wording and readability of some passages of the text. The study design, data analysis, interpretation and the writing of the manuscript are the authors' own work. After using this tool, the authors reviewed and edited the content as needed and take full responsibility for the content of the published article.

Acknowledgements

This work used the National Geochemical Survey of Australia and the Heavy Mineral Map of Australia datasets of Geoscience Australia, the National Geochemical Mapping data of the Geological Survey of India hosted on the AuScope EarthBank platform, and HydroSHEDS hydrological data. We thank colleagues at the John de Laeter Centre, Curtin University, for discussion.

Funding

The AuScope EarthBank project is supported by AuScope, the EarthBank university consortium partners, the Western Australian Government, and the Australian Government through the National Collaborative Research Infrastructure Strategy (NCRIS): auscope.org.au. This research received no other specific grant from any public or private funding agency.

CRediT authorship contribution statement

Bhavik H. Lodhia: Writing – original draft, Visualisation, Methodology, Investigation, Data curation, Conceptualisation, Supervision, Project administration. Princy Agrahari: Writing – review & editing, Data curation. Aditya Priyadarshi: Writing – review & editing, Data curation. Brent I.A. McInnes: Writing – review & editing, Conceptualisation.

Competing interests

The authors declare that they have no known competing financial interests or personal relationships that could have appeared to influence the work reported in this paper.

Data availability

The National Geochemical Survey of Australia and Heavy Mineral Map of Australia datasets are available from Geoscience Australia, the National Geochemical Mapping data from the Geological Survey of India, and the HydroSHEDS drainage data from hydrosheds.org. The analysis code that produced every table and reported statistic in this paper is archived at https://doi.org/10.5281/zenodo.22269835, released under the MIT licence and open on publication. The input datasets are not redistributed with the code, and their providers and access conditions are listed in the repository's data documentation.

Appendix. Catchment geology and raw geochemical data of the analogue samples

Pair	Domain	Area (km²)	Host orogen or craton (%)	Largest mapped unit (%)		Second unit (%)	Dominant era (%)
1	Archaean	2,715	Yilgarn 100.0	Yilgarn Craton granites	56.8	Youanmi Terrane 43.2	100.0
2	Archaean	2,567	Yilgarn 99.8	Youanmi Terrane	87.1	Yilgarn Craton granites 12.6	99.8
3	Archaean	40,592	Yilgarn 98.3	Youanmi Terrane	56.4	Yilgarn Craton granites 37.5	93.9
4	Archaean	3,456	Yilgarn 100.0	Yilgarn Craton granites	74.6	Youanmi Terrane 25.4	100.0
5	Archaean	266	Yilgarn 100.0	Youanmi Terrane	52.5	Yilgarn Craton granites 47.5	100.0
6	Archaean	76,624	Yilgarn 85.9	Yilgarn Craton granites	55.2	Narryer Terrane 15.2	69.2
7	Archaean	41,734	Yilgarn 78.4	Yilgarn Craton granites	47.9	Youanmi Terrane 15.3	64.3
8	Archaean	1,325	Yilgarn 100.0	Youanmi Terrane	88.3	Yilgarn Craton granites 11.7	100.0
9	Archaean	1,630	Yilgarn 100.0	Yilgarn Craton granites	59.4	Youanmi Terrane 40.6	100.0
10	Archaean	5,780	Yilgarn 100.0	Youanmi Terrane	70.4	Yilgarn Craton granites 29.6	100.0
1	Palaeoproterozoic	3,643	Capricorn 93.3	Burringurrah Domain	79.1	Edmund Basin 14.1	93.3
2	Palaeoproterozoic	54,036	Capricorn 84.9	Ashburton Basin	25.3	Edmund Basin 22.2	58.0
3	Palaeoproterozoic	7,235	Halls Creek 55.4	Lamboo Province, Western Zone	55.4	Lennard Shelf 28.6	71.4
4	Palaeoproterozoic	3,643	Capricorn 93.3	Burringurrah Domain	79.1	Edmund Basin 14.1	93.3
5	Palaeoproterozoic	78,756	Capricorn 75.1	Burringurrah Domain	23.8	Edmund Basin 21.1	49.3
6	Palaeoproterozoic	16,860	Capricorn 85.4	Edmund Basin	52.6	Burringurrah Domain 25.2	80.5
7	Palaeoproterozoic	80,796	Capricorn 73.2	Burringurrah Domain	23.1	Edmund Basin 20.4	47.9
8	Palaeoproterozoic	35,381	Capricorn 84.4	Collier Basin	24.5	Edmund Basin 20.1	45.4
9	Palaeoproterozoic	6,006	Capricorn 85.3	Edmund Basin	60.7	Narimbunna Dolerite 14.6	85.2
10	Palaeoproterozoic	42,377	Capricorn 86.8	Burringurrah Domain	25.8	Collier Basin 20.4	50.9

Table 3. Geology drained by each of the twenty analogue catchments, measured as the fraction of catchment area underlain by each unit of the Geological Survey of Western Australia 1:500 000 tectonic units layer [6]. Areas are computed by point counting on a regular grid of approximately 30 000 interior points per catchment, each point weighted by the cosine of its latitude so that the fractions are true areas. The host orogen or craton gives the summed area fraction of the Capricorn or Halls Creek orogens for the Palaeoproterozoic set and of the Yilgarn Craton for the Archaean set, and dominant era gives the summed area fraction of Palaeoproterozoic units for the Palaeoproterozoic set and of Mesoarchaean units for the Archaean set.

The forty samples that define the twenty analogue pairs, one Indian and one Australian per pair, are listed with their identifiers and coordinates in Table 4, and their raw stream-sediment geochemistry in Table 5 (India, National Geochemical Mapping) and Table 6 (Australia, National Geochemical Survey of Australia). Columns are numbered by analogue pair, matching Figures 3 and 4: pairs 1 to 10 are Palaeoproterozoic (Sandmata) and pairs 11 to 20 are Archaean (Mangalwar).

Pair	Domain	India lat	India lon	NGSA site	NGSA sample

Pair	Domain	India lat	India lon	NGSA site	NGSA sample
1	Palaeoproterozoic	25.259	74.339	2007190003	2007190003001
2	Palaeoproterozoic	25.563	74.689	2007191253	2007191253001
3	Palaeoproterozoic	25.458	74.669	2007190966	2007190966001
4	Palaeoproterozoic	25.527	74.456	2007190213	2007190213001
5	Palaeoproterozoic	25.259	74.359	2007190541	2007190541001
6	Palaeoproterozoic	25.226	74.320	2007191419	2007191419001
7	Palaeoproterozoic	25.709	74.899	2007191192	2007191192001
8	Palaeoproterozoic	25.226	74.400	2007191503	2007191503001
9	Palaeoproterozoic	25.440	74.669	2007191003	2007191003001
10	Palaeoproterozoic	25.581	74.899	2007191392	2007191392001
11	Archaean	26.527	75.500	2007190230	2007190230001
12	Archaean	25.691	74.456	2007190973	2007190973001
13	Archaean	26.027	74.840	2007190287	2007190287001
14	Archaean	26.136	75.250	2007191335	2007191335001
15	Archaean	24.063	73.858	2007190855	2007190855001
16	Archaean	24.081	73.877	2007190039	2007190039001
17	Archaean	26.100	75.170	2007191462	2007191462001
18	Archaean	25.422	74.339	2007191159	2007191159001
19	Archaean	26.740	75.880	2007190244	2007190244001
20	Archaean	26.045	74.731	2007190914	2007190914001

Table 4. Identifiers and coordinates of the forty analogue samples. India samples (National Geochemical Mapping) are identified by latitude and longitude; Australia samples by National Geochemical Survey of Australia site and sample number. The value reported for each Australian site in Table 6 is the median of the analyses of the two size fractions at both sampling depths, as described in Section 2.1.

Variable	1	2	3	4	5	6	7	8	9	10	11	12	13	14	15	16	17	18	19	20
SiO2 (wt%)	60.91	62.35	65.32	64.71	60.23	63.18	59.70	65.51	68.07	65.22	72.63	54.00	64.97	64.80	62.51	63.49	65.85	62.05	76.97	62.89
TiO2 (wt%)	0.92	0.89	1.04	1.02	0.75	1.00	0.85	2.01	0.84	0.90	0.69	1.13	0.90	0.89	0.71	0.79	0.88	1.16	0.40	1.10
Al2O3 (wt%)	14.34	12.15	10.51	13.93	15.00	13.50	12.99	11.41	11.57	13.07	10.14	14.90	13.35	14.88	16.13	16.58	14.38	13.63	8.66	13.94
Fe2O3 (wt%)	5.43	5.89	6.88	5.97	5.18	5.38	5.60	6.52	5.23	5.51	3.05	6.62	5.38	5.32	5.23	5.44	5.22	6.97	2.17	6.87
MnO (wt%)	0.07	0.08	0.19	0.10	0.06	0.10	0.07	0.11	0.12	0.08	0.06	0.09	0.07	0.08	0.07	0.12	0.07	0.10	0.04	0.08
MgO (wt%)	2.29	2.48	1.85	2.26	2.09	1.89	1.97	1.59	1.88	1.96	1.59	3.18	2.12	2.53	2.47	2.34	2.24	2.34	1.04	1.98
CaO (wt%)	2.05	4.04	2.56	2.48	1.96	2.56	1.63	3.70	2.29	1.96	3.04	4.45	2.41	2.06	1.48	1.13	2.05	2.76	1.03	2.23
Na2O (wt%)	1.65	1.41	1.28	1.27	1.26	1.89	0.99	1.39	1.82	1.36	1.42	1.30	1.04	0.70	1.82	1.41	1.13	1.61	1.23	1.16
K2O (wt%)	2.70	2.06	1.73	2.50	2.95	2.43	1.99	1.59	1.97	1.93	1.94	2.43	2.47	2.11	3.56	3.33	2.61	2.13	1.34	2.71
P2O5 (wt%)	0.09	0.13	0.08	0.11	0.12	0.10	0.08	0.08	0.11	0.10	0.09	0.13	0.15	0.09	0.11	0.10	0.10	0.15	0.06	0.19
Sc (ppm)	13.0	9.0	9.0	13.0	11.0	14.0	8.0	13.0	7.0	9.0	9.0	16.0	11.0	13.0	12.0	11.0	12.0	14.0	9.0	13.0
V (ppm)	83.0	113.0	133.0	81.0	80.0	83.0	84.0	110.0	107.0	69.0	59.0	112.0	94.0	84.0	80.0	82.0	79.0	103.0	41.0	115.0
Cr (ppm)	108.0	90.0	101.0	73.0	99.0	85.0	100.0	103.0	91.0	107.0	92.0	104.0	100.0	113.0	78.0	93.0	92.0	147.0	33.0	74.0
Co (ppm)	13.0	16.0	17.0	16.0	13.0	15.0	15.0	18.0	13.0	14.0	18.0	19.0	26.0	19.0	21.0	16.0	20.0	19.0	19.0	31.0
Ni (ppm)	31.0	24.0	17.0	36.0	35.0	28.0	34.0	32.0	14.0	35.0	31.0	37.0	37.0	47.0	34.0	30.0	36.0	41.0	27.0	38.0
Cu (ppm)	36.0	18.0	66.0	26.0	35.0	20.0	25.0	18.0	13.0	26.0	21.0	21.0	20.0	24.0	24.0	26.0	24.0	38.0	20.0	19.0
Zn (ppm)	56.0	62.0	244.0	67.0	65.0	55.0	79.0	65.0	72.0	67.0	44.0	64.0	76.0	62.0	86.0	63.0	64.0	86.0	37.0	71.0
Ga (ppm)	19.0	16.0	13.0	16.0	21.0	16.0	19.0	16.0	13.0	17.0	19.0	16.0	25.0	23.0	16.0	22.0	24.0	20.0	14.0	20.0
Rb (ppm)	–	–	–	–	–	–	–	–	–	–	–	–	–	–	–	–	–	–	–	–
Sr (ppm)	115.0	162.0	85.0	179.0	126.0	134.0	135.0	146.0	120.0	173.0	179.0	169.0	141.0	124.0	102.0	103.0	138.0	144.0	125.0	134.0
Y (ppm)	43.0	32.0	30.0	89.0	52.0	49.0	36.0	57.0	30.0	44.0	31.0	60.0	36.0	34.0	24.0	24.0	40.0	42.0	18.0	44.0
Zr (ppm)	550.0	440.0	453.0	639.0	397.0	489.0	563.0	919.0	525.0	682.0	417.0	726.0	658.0	462.0	185.0	242.0	682.0	492.0	299.0	513.0
Nb (ppm)	17.00	12.00	9.00	26.00	16.00	25.00	17.00	33.00	11.00	17.00	15.00	21.00	16.00	14.00	14.00	15.00	16.00	24.00	10.00	16.00
Cs (ppm)	5.0	5.0	11.0	5.0	5.0	10.0	5.0	12.0	5.0	5.0	3.8	5.0	–	4.9	4.9	6.0	4.1	10.0	2.7	–
Ba (ppm)	434.0	446.0	362.0	541.0	413.0	365.0	454.0	355.0	448.0	432.0	386.0	420.0	527.0	355.0	351.0	350.0	462.0	380.0	327.0	707.0
La (ppm)	146.1	75.8	140.4	156.8	171.7	206.8	89.9	272.6	98.1	154.8	54.4	111.7	114.7	75.0	66.4	108.5	140.1	104.5	43.7	73.2
Ce (ppm)	274.4	158.2	259.9	290.6	318.9	413.4	170.0	481.1	177.7	278.8	101.3	211.1	211.8	143.9	120.9	198.2	275.6	198.7	81.8	132.3
Pr (ppm)	30.3	17.5	29.1	31.6	41.1	46.5	18.9	53.3	19.5	31.4	12.2	24.0	25.9	16.6	14.1	22.7	32.5	22.3	9.4	15.9
Nd (ppm)	115.9	67.5	112.4	120.8	133.5	172.1	72.0	204.0	74.1	120.0	46.4	91.3	101.6	63.7	54.9	87.5	123.3	89.7	36.0	64.6
Sm (ppm)	21.4	12.0	20.3	22.0	24.0	31.0	12.6	36.4	13.2	21.1	8.2	14.9	15.8	11.5	9.9	15.2	20.4	16.5	6.2	12.1
Eu (ppm)	3.00	1.93	2.55	2.65	2.92	3.39	1.94	4.21	1.96	2.29	1.27	2.71	1.91	1.79	1.54	2.40	2.09	2.40	1.07	2.27
Gd (ppm)	19.4	10.5	15.9	19.8	21.6	25.3	10.1	29.9	11.3	15.7	6.5	12.5	12.0	8.5	7.8	12.2	15.0	15.1	5.0	10.3
Tb (ppm)	2.83	1.65	2.58	2.87	3.16	4.00	1.52	4.64	1.80	2.46	1.13	2.18	1.74	1.46	1.20	1.67	2.16	2.32	0.77	1.76
Dy (ppm)	13.6	8.3	12.5	13.7	15.3	18.6	7.0	20.9	8.8	11.0	6.6	9.5	7.9	6.8	5.4	7.2	9.8	12.0	4.0	9.5
Ho (ppm)	2.60	1.68	2.45	2.68	2.97	3.52	1.44	3.94	1.79	2.16	1.16	1.98	1.39	1.22	0.93	1.20	1.63	2.47	0.71	1.70
Er (ppm)	6.5	4.5	6.4	6.8	7.5	9.0	4.1	10.7	4.8	6.0	3.5	4.9	4.2	3.8	2.9	3.6	4.7	6.3	2.1	5.2
Yb (ppm)	6.3	4.4	6.0	6.5	7.3	8.3	3.8	9.6	4.8	5.7	3.5	4.6	3.9	3.8	2.5	3.1	4.0	6.2	2.3	5.1
Lu (ppm)	0.88	0.63	0.87	0.93	1.00	1.17	0.54	1.33	0.68	0.82	0.53	0.95	0.55	0.59	0.36	0.45	0.65	0.86	0.32	0.74
Hf (ppm)	16.88	14.13	17.73	16.47	8.99	17.19	18.96	27.87	15.58	21.10	17.83	12.91	17.44	18.48	5.75	8.42	27.48	12.21	11.21	17.71
Ta (ppm)	1.69	1.33	1.93	1.43	1.23	4.17	1.22	3.16	1.31	1.48	1.28	0.86	1.28	1.50	1.41	2.13	1.44	1.98	1.07	1.39
Pb (ppm)	28.0	9.0	71.0	23.0	29.0	31.0	21.0	25.0	23.0	21.0	20.0	17.0	17.0	17.0	29.0	21.0	18.0	20.0	25.0	14.0
Th (ppm)	33.00	11.00	21.00	35.00	38.00	44.00	25.00	56.00	17.00	45.00	16.00	27.00	42.00	15.00	21.00	24.00	37.00	25.00	8.00	15.00
U (ppm)	9.75	4.62	7.88	7.47	11.13	12.93	3.64	16.11	5.15	7.14	3.76	3.29	3.84	3.81	4.42	4.60	4.59	4.80	2.94	2.62

Table 5. Raw stream-sediment geochemistry of the twenty north-west Indian (National Geochemical Mapping) analogue samples, one per analogue pair (columns 1–20; pairs 1–10 Palaeoproterozoic/Sandmata, 11–20 Archaean/Mangalwar; numbering as in Figures 3 and 4). Major elements as oxide wt%, trace elements in parts per million. Sample coordinates are listed in Table 4.

Variable	1	2	3	4	5	6	7	8	9	10	11	12	13	14	15	16	17	18	19	20
Si (ppm)	358084.5	311475.0	316525.5	359910.0	299012.0	325736.0	309407.5	320311.5	332681.5	326897.0	304247.0	274032.0	213026.5	264165.5	277322.0	319673.5	310622.5	359884.0	248764.0	293973.5
Ti (ppm)	4449.5	6490.5	4698.5	4587.5	6607.5	7146.5	5064.5	5687.0	5837.5	5735.0	9834.5	4524.5	5705.0	3554.0	5678.5	4582.0	3683.0	3739.5	5079.0	5879.5
Al (ppm)	51035.0	57532.0	69873.0	50201.5	78963.5	58228.0	71670.0	64881.5	49010.5	67430.0	76476.0	102462.0	91209.0	88226.5	102726.5	75875.0	67946.0	52604.5	100300.0	81665.5
FeT (ppm)	33431.5	68181.0	37547.0	33519.0	48440.5	45027.0	42118.0	50531.5	45559.0	41985.0	56204.0	53193.0	46041.5	40383.5	55515.0	43289.5	38932.0	34141.0	55137.5	62537.0
Mn (ppm)	507.5	747.5	534.5	519.0	670.0	635.5	542.5	604.0	654.5	557.5	1014.5	565.5	333.0	422.0	848.0	577.0	523.0	290.5	658.0	817.0
Mg (ppm)	4287.5	8813.0	5231.0	4218.0	7643.0	7194.0	7320.5	5222.0	7908.5	6238.0	4748.5	5381.5	29815.5	8966.5	1881.5	5104.5	9337.5	5544.5	17716.5	5852.0
Ca (ppm)	4888.5	7665.0	8065.5	4995.5	7036.0	9016.0	9734.5	12725.0	11717.5	7032.5	2401.5	2866.0	8205.0	19475.5	1182.5	2548.0	8394.0	1761.5	4871.0	6268.0
Na (ppm)	5905.5	2960.5	5760.5	5749.5	6955.5	6573.5	7445.0	7923.5	4696.0	6792.0	2040.0	1079.5	19805.0	1001.5	1020.5	2437.0	4151.0	2645.0	2010.5	4050.5
K (ppm)	18370.0	15273.5	22711.5	18200.0	17826.5	17258.0	19574.0	18959.5	15481.5	15365.5	10488.5	10488.0	25405.0	10671.0	11945.5	16083.5	16357.0	12140.5	11534.5	11683.5
P (ppm)	316.0	371.0	303.0	312.0	362.5	395.0	536.5	508.5	397.0	344.5	277.0	332.0	349.0	242.0	489.0	353.5	251.0	251.0	294.5	449.5
Sc (ppm)	11.0	14.0	13.2	11.7	17.1	14.0	12.9	11.9	11.1	12.9	14.7	15.6	16.8	14.0	18.8	16.0	12.3	9.8	17.2	19.2
V (ppm)	73.2	144.6	74.1	77.3	120.5	118.3	102.2	102.6	115.9	94.2	180.4	113.8	105.8	94.1	132.4	113.8	104.9	84.3	119.8	156.8
Cr (ppm)	56.2	125.5	50.7	61.6	91.8	75.2	81.7	75.1	67.2	79.2	141.1	191.6	108.8	110.3	203.5	115.2	124.1	139.4	149.3	258.3
Co (ppm)	8.9	17.8	14.7	9.0	13.6	12.1	11.8	10.8	13.9	10.3	18.1	16.9	18.1	13.8	22.6	13.6	12.2	7.7	18.6	26.9
Ni (ppm)	19.0	40.0	22.2	20.7	29.8	25.8	23.4	19.8	24.9	25.4	35.8	54.5	42.3	36.0	51.3	33.3	33.2	22.3	54.7	78.3
Cu (ppm)	21.2	40.4	26.6	21.1	30.0	28.1	26.6	19.6	26.8	21.0	25.9	40.4	37.8	33.7	46.6	30.1	28.6	23.4	39.6	67.2
Zn (ppm)	39.2	81.5	55.9	41.9	52.8	51.6	56.5	45.4	60.9	45.8	51.0	62.2	53.7	64.8	83.8	60.7	50.8	38.5	67.4	76.0
Ga (ppm)	11.6	15.2	17.6	13.2	18.6	16.2	17.2	14.7	12.1	14.7	17.6	23.4	20.4	20.9	25.0	19.2	17.9	14.0	23.8	19.2
Rb (ppm)	101.0	87.6	153.5	101.7	99.8	96.4	101.1	98.0	96.9	87.6	63.6	76.3	120.5	65.8	85.4	99.0	86.6	53.6	81.6	81.8
Sr (ppm)	79.4	60.2	89.6	86.4	97.2	111.2	109.2	140.9	63.3	83.8	47.2	47.0	88.8	49.8	47.4	68.8	91.8	40.5	62.8	61.1
Y (ppm)	24.9	28.2	37.5	29.0	46.7	35.9	30.5	35.4	30.4	37.0	27.1	23.8	31.9	18.2	23.1	25.3	19.6	14.6	18.3	30.4
Zr (ppm)	438.7	276.2	395.9	507.4	1022.7	649.2	426.1	579.0	355.4	652.9	301.8	192.3	160.7	154.9	267.1	355.1	387.2	235.1	163.9	312.0
Nb (ppm)	11.35	12.30	14.20	12.05	19.50	19.45	15.95	19.20	12.80	16.50	13.40	10.35	14.80	8.60	13.30	14.05	9.85	8.85	11.05	12.55
Cs (ppm)	3.9	5.2	7.2	3.9	3.9	4.1	3.8	2.9	4.5	3.3	2.9	3.6	5.0	3.3	4.0	3.5	2.6	1.7	3.9	3.4
Ba (ppm)	420.5	335.6	552.5	428.4	505.3	414.2	522.9	667.7	335.8	438.5	333.0	257.2	187.3	207.4	330.2	540.5	580.2	350.6	209.6	332.1
La (ppm)	33.1	29.8	47.2	35.9	63.4	50.3	39.9	52.3	35.4	51.9	28.5	31.1	48.3	22.2	36.3	41.3	41.2	21.1	24.7	28.8
Ce (ppm)	60.2	58.4	91.2	65.3	123.5	95.1	78.9	108.6	65.2	102.7	58.1	52.6	95.2	45.9	74.3	78.0	76.8	38.1	53.7	55.1
Pr (ppm)	6.9	6.5	10.4	7.4	13.1	11.2	8.8	11.3	7.6	11.0	5.8	6.0	9.8	4.6	7.1	7.8	7.7	4.3	4.9	6.2
Nd (ppm)	25.6	25.6	39.2	27.6	48.9	39.5	33.0	42.9	28.1	41.9	21.7	20.0	35.6	17.3	25.3	27.8	25.6	14.6	17.7	24.1
Sm (ppm)	5.2	5.2	8.1	5.5	9.8	8.2	6.6	8.8	5.7	8.4	4.6	3.8	7.1	3.5	5.3	5.6	5.0	3.6	3.5	5.2
Eu (ppm)	0.88	1.03	1.37	0.84	1.48	1.24	1.27	1.33	1.05	1.31	0.92	0.89	1.17	0.75	1.05	1.04	0.74	0.62	0.76	1.14
Gd (ppm)	4.0	4.4	6.4	4.1	7.6	6.3	5.5	6.3	4.7	6.4	4.1	3.8	5.7	3.0	4.1	4.4	3.9	3.0	3.1	4.5
Tb (ppm)	0.70	0.66	1.12	0.67	1.28	1.09	0.77	0.97	0.82	1.00	0.71	0.59	0.95	0.45	0.73	0.77	0.67	0.55	0.52	0.84
Dy (ppm)	3.8	4.3	6.1	4.1	7.2	5.9	4.5	5.7	4.1	5.4	4.2	3.5	5.2	3.0	3.7	4.1	3.7	3.3	2.9	4.8
Ho (ppm)	0.80	0.82	1.22	0.80	1.48	1.22	1.01	1.07	0.91	1.17	0.87	0.71	1.04	0.56	0.80	0.80	0.71	0.60	0.58	1.00
Er (ppm)	2.3	2.6	3.5	2.4	4.3	3.4	2.9	3.2	2.6	3.4	2.5	2.0	2.8	1.6	2.4	2.3	1.9	1.7	1.8	2.9
Yb (ppm)	2.5	2.7	3.5	2.7	4.8	3.6	2.9	3.5	2.7	3.6	2.8	2.1	2.7	1.8	2.5	2.4	2.1	1.8	1.9	3.1
Lu (ppm)	0.40	0.31	0.54	0.33	0.69	0.53	0.42	0.41	0.39	0.46	0.38	0.27	0.37	0.23	0.39	0.35	0.30	0.27	0.23	0.49
Hf (ppm)	11.22	7.64	10.79	12.98	25.96	16.50	11.10	15.76	9.06	16.43	7.92	5.22	4.55	4.21	7.57	9.00	10.08	6.59	4.38	8.55
Ta (ppm)	1.15	1.04	1.08	1.00	1.43	1.36	1.28	1.31	1.06	1.32	1.21	0.86	1.24	1.31	1.15	1.13	0.72	0.83	0.94	1.29
Pb (ppm)	21.3	19.4	24.5	21.1	26.0	20.1	23.4	23.9	20.6	24.1	21.2	21.9	21.4	16.6	29.0	27.5	19.4	17.0	20.1	20.5
Th (ppm)	15.99	13.57	19.50	16.64	30.94	25.05	19.27	23.57	15.26	27.96	17.07	18.30	29.76	12.88	22.13	22.60	18.93	10.61	12.21	16.54
U (ppm)	3.50	2.87	5.12	3.35	5.63	4.00	3.41	4.75	3.29	5.02	2.51	2.89	9.73	2.50	5.88	4.65	3.29	3.20	18.77	4.85

Table 6. Raw stream-sediment geochemistry of the twenty Western Australian (National Geochemical Survey of Australia) analogue samples, one per analogue pair (columns 1–20, matched to Table 5). All values in parts per million, each the median of the analyses of the two size fractions at both sampling depths. Total iron is reported by the survey as FeT and is determined by X-ray fluorescence on the same total suite as the other major elements. Site identifiers are listed in Table 4.

Fingerprint	Pairs	Spearman rho	Corrected q	Leave-one-out range of rho	Refits still clearing q < 0.05	Bootstrap 95% interval on rho
Light rare earths, monazite-associated	20	0.696	0.004	0.649 to 0.753	20 of 20	0.363 to 0.871
Heavy rare earths, host not resolved	20	0.506	0.059	0.424 to 0.571	9 of 20	0.030 to 0.796
Zirconium and hafnium, zircon-associated	20	0.313	0.300	0.237 to 0.458	0 of 20	-0.165 to 0.716
Titanium, titanium-oxide-associated	20	-0.240	0.382	-0.309 to -0.131	0 of 20	-0.630 to 0.199
Phosphorus, apatite-associated	20	0.130	0.585	0.047 to 0.280	0 of 20	-0.379 to 0.638
Light rare earths, monazite-associated	19	0.716	0.004	0.670 to 0.785	19 of 19	0.366 to 0.897
Heavy rare earths, host not resolved	19	0.561	0.035	0.483 to 0.640	12 of 19	0.081 to 0.845
Zirconium and hafnium, zircon-associated	19	0.277	0.414	0.195 to 0.422	0 of 19	-0.206 to 0.700
Titanium, titanium-oxide-associated	19	-0.216	0.465	-0.294 to -0.098	0 of 19	-0.628 to 0.264
Phosphorus, apatite-associated	19	0.122	0.613	0.039 to 0.278	0 of 19	-0.407 to 0.639

Table 7. Stability of the fingerprint transfer correlations under resampling. Leave one out testing drops each analogue pair in turn and refits, recomputing the Benjamini-Hochberg correction across the five fingerprints at every refit, so the fourth column counts how many refits would still declare that fingerprint transferable. The bootstrap resamples the pairs with replacement 10 000 times and reports the 2.5 and 97.5 percentiles, and Fisher intervals computed analytically are given for comparison in the results file, agreeing closely with the bootstrap for the strongest correlation, the light rare-earth fingerprint, and being narrower than the bootstrap for the weak correlations, where the bootstrap is the more conservative of the two. The twenty pairs are not twenty independent catchments, because Palaeoproterozoic pairs 1 and 4 share a catchment, so the analysis is repeated with that duplicate removed. The light rare-earth signature is stable under every test and in both variants, whereas the heavy rare-earth signature clears the threshold at nineteen pairs but not at twenty.

Matching variant	Pairs	Shared with published set	Light rare earths (Ce, Nd, Pr)	Heavy rare earths (Dy)	Zircon (Zr, Hf)	Titanium oxides (Ti)	Apatite (P)
Mutual nearest neighbour, ten pairs per domain (published)	20	20	0.70*	0.51	0.31	−0.24	0.13
One-directional nearest neighbour, mutuality not required	20	20	0.70*	0.51	0.31	−0.24	0.13
Greedy unique assignment, each Indian catchment used once	20	20	0.70*	0.51	0.31	−0.24	0.13
Globally optimal one-to-one assignment	20	20	0.70*	0.51	0.31	−0.24	0.13
Mahalanobis distance in place of Euclidean	20	4	0.67*	0.57*	0.45	0.32	−0.10
All mutual pairs, no distance ranking cap	48	20	0.54*	0.38*	0.32*	−0.10	−0.04
Five pairs per domain	10	10	0.67	0.42	−0.21	−0.61	0.68
Eight pairs per domain	16	16	0.66*	0.43	0.12	−0.29	−0.09
Twelve pairs per domain	24	20	0.74*	0.57*	0.42	−0.10	−0.08
Fifteen pairs per domain	30	20	0.72*	0.54*	0.41*	0.03	−0.03
Twenty pairs per domain	40	20	0.54*	0.37*	0.37*	0.08	0.07
Thirty pairs per domain	60	20	0.54*	0.42*	0.30*	−0.06	0.03
Mutual pairs within the 25th distance percentile	22	18	0.67*	0.36	0.29	−0.35	−0.30
Mutual pairs within the 50th distance percentile	32	20	0.71*	0.50*	0.42*	−0.03	0.00

Matching variant	Pairs	Shared with published set	Light rare earths (Ce, Nd, Pr)	Heavy rare earths (Dy)	Zircon (Zr, Hf)	Titanium oxides (Ti)	Apatite (P)
Mutual pairs within the 75th distance percentile	42	20	0.57*	0.37*	0.34*	0.04	0.14
Random analogue control, mean of 10 000 draws	20		0.08	0.18	0.02	0.08	−0.04
Random analogue control, 95th percentile	20		0.44	0.53	0.40	0.45	0.35

Table 8. Sensitivity of the fingerprint transfer to the matching procedure. Each row repeats the transfer test on a different set of analogue pairs and gives the Spearman rank correlation for each fingerprint, an asterisk marking a corrected q-value below 0.05 within that row, with the Benjamini-Hochberg correction recomputed across the five fingerprints for every variant, and the third column giving how many of the twenty published pairs the variant reproduces. Requiring only one-directional nearest neighbours, pairing greedily so that each Indian site is used once, and solving for the globally optimal one-to-one assignment each return the same twenty pairs as the published mutual nearest neighbour rule, so their correlations are identical to it, whereas substituting Mahalanobis for Euclidean distance selects a largely different set, sharing four pairs, and returns the same result. The last two rows pair Indian and Australian catchments at random within the same domains 10 000 times and give the mean and the 95th percentile of the resulting correlations, the observed light rare-earth correlation being matched or exceeded by 0.1% of these random draws, against 6.5% for the heavy rare-earth fingerprint, 10.5% for zircon, 24.3% for apatite and 91.7% for the titanium oxides. Correlations computed on more pairs are more easily resolved, so the heavy rare-earth and zircon fingerprints clear the threshold in the larger variants, the number of retained pairs setting the statistical power without changing the ranking of the fingerprints.

Fingerprint elements	Measured mineral	Sites in pool	rho (pool)	p (pool)	Analogue pairs	rho (pairs)	p (pairs)
Ce, Nd, Pr (as published)	Monazite	83	0.581	<0.001	19	0.551	0.016
Ce	Monazite	83	0.626	<0.001	19	0.575	0.011
La, Ce, Pr, Nd, Sm	Monazite	83	0.575	<0.001	19	0.551	0.016
Ce, Nd, Pr, Th	Monazite	83	0.631	<0.001	19	0.602	0.007
Ce, Nd, Pr, Th, P	Monazite	83	0.544	<0.001	19	0.581	0.010
La, Ce, Ca	Allanite	46	0.455	0.002	15	0.532	0.043
Dy (as published)	Xenotime	77	0.046	0.690	19	−0.356	0.134
Y	Xenotime	77	0.022	0.850	19	−0.302	0.206
Y, Dy	Xenotime	77	0.041	0.723	19	−0.307	0.200
Dy, Ho, Er, Yb, Lu	Xenotime	77	0.005	0.964	19	−0.300	0.209
Y, Dy, Ho, Er, Yb, Lu	Xenotime	77	0.010	0.934	19	−0.309	0.195
Zr, Hf	Zircon	85	0.169	0.123	20	−0.014	0.957
Ti	Ilmenite	85	−0.184	0.092	20	−0.414	0.072
P	Apatite	69	0.209	0.087	17	0.218	0.397

Table 9. Mineralogical validation of the pathfinder fingerprints against measured heavy-mineral grain counts. The Heavy Mineral Map of Australia grain counts are made on the National Geochemical Survey of Australia samples themselves, so each fingerprint score is compared with the measured abundance of its candidate host mineral at the same site with no spatial matching involved. Scores are computed as in Equation 5, and correlations are Spearman rank correlations with permutation probabilities from 100 000 relabellings, evaluated over the drainage-selected Australian pool and over the analogue pairs, with sample numbers differing between rows because a site enters a row only where both the elements and the host mineral are reported there. The first five rows vary the element combination used for the light rare-earth fingerprint, the sixth tests the combination diagnostic of allanite, and the five heavy rare-earth rows include the combinations most commonly used for xenotime.

References

Ahmad, I., Mondal, M. E. A., Bhutani, R., and Satyanarayanan, M. (2018). Geochemical evolution of the Mangalwar Complex, Aravalli Craton, NW India: insights from elemental and Nd-isotope geochemistry of the basement gneisses. *Geoscience Frontiers*, 9:931–942. https://doi.org/10.1016/j.gsf.2017.07.003

Aitken, A. R. A., Joly, A., Dentith, M. C., Johnson, S. P., Thorne, A. M., and Tyler, I. M. (2014). 3D architecture, structural evolution, and mineral prospectivity of the Gascoyne Province. Geological Survey of Western Australia, Report 123, 94 pp.

Albanese, A., Bowen, C., and King, M. (2026). Collaborating with India on energy and resources . Media release, Prime Minister of Australia, 9 July 2026. Available at https://www.pm.gov.au/media/collaborating-india-energy-and-resources (accessed 21 July 2026).

Bagchi, J., Dubey, J., Shimyaphy, R. V., and Singh, N. (2021). Signatures of Heavy Metal concentration over Laterites identified through Regional Stream Sediment Geochemical Survey in parts of Katni, Panna and Satna Districts of Madhya Pradesh, India. *Journal of the Geological Society of India*, 97:481–490. https://doi.org/10.1007/s12594-021-1714-2

Benjamini, Y. and Hochberg, Y. (1995). Controlling the false discovery rate: a practical and powerful approach to multiple testing. *J. R. Statist. Soc. B*, 57, 289–300.

Boone, S. C., Dalton, H., Prent, A., Kohlmann, F., Theile, M., Gréau, Y., Florin, G., Noble, W., Hodgekiss, S. A., Ware, B., Phillips, D., Kohn, B., O'Reilly, S., Gleadow, A., McInnes, B., and Rawling, T. (2022). AusGeochem: An Open Platform for Geochemical Data Preservation, Dissemination and Synthesis. *Geostandards and Geoanalytical Research*, 46:245–259. https://doi.org/10.1111/ggr.12419

Boone, S. C., Kohlmann, F., Noble, W., Theile, M., Beucher, R., Kohn, B., Glorie, S., Danišík, M., Zhou, R., McMillan, M., Nixon, A., Gleadow, A., Qin, X., Müller, D., and McInnes, B. (2023). A geospatial platform for the tectonic interpretation of low-temperature thermochronology Big Data. *Scientific Reports*, 13. https://doi.org/10.1038/s41598-023-35776-3

Cawood, P. A. and Tyler, I. M. (2004). Assembling and reactivating the Proterozoic Capricorn Orogen: lithotectonic elements, orogenies, and significance. *Precambrian Research*, 128:201–218.

Chivas, A. R., Bourman, R. P., Buckman, S., Dux, F. W., Wheeler, D., and Karamiqucham, B. (2019). Antiquity of the giant inselberg Burringurrah (Mount Augustus), Western Australia, inferred from oxygen isotope dating of kaolinitic weathering. *Geomorphology*, 328:108–117. https://doi.org/10.1016/j.geomorph.2018.12.005

Cutten, N., Martin, D., and Riganti, A. (2022). 1:500,000 tectonic units of Western Australia.

de Caritat, P. and Cooper, M. (2016). A continental-scale geochemical atlas for resource exploration and environmental management: The national geochemical survey of Australia. *Geochemistry: Exploration, Environment, Analysis*, 16:3–13. https://doi.org/10.1144/geochem2014-322

de Caritat, P., McInnes, B. I., Walker, A. T., Bastrakov, E., Rowins, S. M., and Prent, A. M. (2022). The Heavy Mineral Map of Australia: Vision and Pilot Project. *Minerals*, 12:961. https://doi.org/10.3390/min12080961

de Caritat, P., Walker, A. T., Bastrakov, E., Main, P., and McInnes, B. I. A. (2023). The Heavy Mineral Map of Australia project final data release: national dataset and atlas. Geoscience Australia Record 2023/42 (eCat 148916).

Deb, M. (2014). Precambrian geodynamics and metallogeny of the Indian shield. *Ore Geology Reviews*, 57:1–28. https://doi.org/10.1016/j.oregeorev.2013.08.022

Fareeduddin and Banerjee, D. M. (2020). Aravalli Craton and its mobile belts: An update. *Episodes*, 43:88–108. https://doi.org/10.18814/epiiugs/2020/020005

Geological Survey of India (2014). Standard Operating Procedure for National Geochemical Mapping & Quality Management. Technical report.

Geological Survey of Western Australia (2026). MINEDEX Database. Department of Mines, Industry Regulation and Safety, Western Australia, digital data, GDA2020, extracted 29 June 2026. Licence CC-BY-4.0.

Ghosh, S., Cogné, N., Prabhakar, N., Sheth, H., and Mishra, D. (2026). Late Palaeoproterozoic TTG gneisses in the Sandmata Complex, Aravalli Craton, and their significance for the geodynamics and crustal growth of northwestern India. *Lithos*, 540-541. https://doi.org/10.1016/j.lithos.2026.108659

Ghosh, S., D'Souza, J., Goud, B. R., and Prabhakar, N. (2022). A review of the Precambrian tectonic evolution of the Aravalli Craton, northwestern India: Structural, metamorphic and geochronological perspectives from the basement complexes and supracrustal sequences. *Earth-Science Reviews*, 232. https://doi.org/10.1016/j.earscirev.2022.104098

Grunsky, E., de Caritat, P., Arne, D., Caciagli, N., and Scher, S. (2026). A Workflow for the Analysis of Multivariate Exploration Geochemical Data. *Geochemistry: Exploration, Environment, Analysis*. https://doi.org/10.1144/geochem2025-077

Grunsky, E. C. (2010). The interpretation of geochemical survey data. *Geochemistry: Exploration, Environment, Analysis*, 10:27–74. https://doi.org/10.1144/1467-7873/09-210

Grunsky, E. C. and de Caritat, P. (2020). State-of-the-art analysis of geochemical data for mineral exploration. *Geochemistry: Exploration, Environment, Analysis*, 20:217–232. https://doi.org/10.1144/geochem2019-031

Guha, D. B., Raza, A., Neogi, S., and Korakoppa, M. (2020). Allanite-britholite bearing migmatite gneiss-Amet Granite and intrusive syenite-monzonite rocks of SW Rajasthan, India, and their REE potential. *Episodes*, 43:665–674. https://doi.org/10.18814/epiiugs/2020/020044

Heseldell, L. J., Timms, N. E., Olierook, H. K., Smail, T. E., Clark, C., Conner, G., and Makin, S. (2025). Petrogenesis and geochronology of the granulite facies gneissic suite hosting the Katanning Gold Deposit, Yilgarn Craton, Southwest Western Australia. *Precambrian Research*, 426. https://doi.org/10.1016/j.precamres.2025.107803

Ivanic, T. J., Belousova, E. A., Kirkland, C. L., Kranendonk, M. J. V., Wingate, M. T. D., and Wyche, S. (2013). *Juvenile crust formation and recycling in the Northern Murchison domain, Yilgarn Craton: evidence from Hf isotopes and granite geochemistry*. Geological Survey of Western Australia.

Ivanic, T. J., Van Kranendonk, M. J., Kirkland, C. L., Wyche, S., Wingate, M. T. D., and Belousova, E. A. (2012). Zircon Lu–Hf isotopes and granite geochemistry of the Murchison Domain of the Yilgarn Craton: evidence for reworking of Eoarchean crust during Meso-Neoarchean plume-driven magmatism. *Lithos*, 148:112–127. https://doi.org/10.1016/j.lithos.2012.06.006

Johnson, S. P., Thorne, A. M., Tyler, I. M., Korsch, R. J., Kennett, B. L. N., Cutten, H. N., Goodwin, J., Blay, O., Blewett, R. S., Joly, A., Dentith, M. C., Aitken, A. R. A., Holzschuh, J., Salmon, M., Reading, A., Heinson, G., Boren, G., Ross, J., Costelloe, R. D., and Fomin, T. (2013). Crustal architecture of the Capricorn Orogen, Western Australia and associated metallogeny. *Australian Journal of Earth Sciences*, 60:681–705. https://doi.org/10.1080/08120099.2013.826735

Korhonen, F.J., Blereau, E.R., Kelsey, D.E., Fielding, I.O.H. and Romano, S.S., (2021), Metamorphic evolution of the southwest Yilgarn: Geological Survey of Western Australia, digital data layer. GSWA metamorphic evolution of the SW Yilgarn.

Lehner, B. and Grill, G. (2013). Global river hydrography and network routing: Baseline data and new approaches to study the world's large river systems. *Hydrological Processes*, 27:2171–2186. https://doi.org/10.1002/hyp.9740

Martin, D., Hocking, R., Riganti, A., and Tyler, I. (2015). Geological map of Western Australia 1:2 500 000, 2015 . Technical report, Geological Survey of Western Australia.

McDonough, W. F. and Sun, S.-s. (1995). The composition of the Earth. *Chemical Geology*, 120:223–253. https://doi.org/10.1016/0009-2541(94)00140-4

McLennan, S. M., Hemming, S., McDaniel, D. K., and Hanson, G. N. (1993). *Geochemical approaches to sedimentation, provenance, and tectonics*. Geological Society of America. https://doi.org/10.1130/SPE284

Myers, J. S. (1995). *The generation and assembly of an Archaean supercontinent: evidence from the Yilgarn craton, Western Australia*, volume 95, pages 143–154. Geological Society of London Special Publication.

Naushad, M., Dongre, A., Behera, J. R., Murthy, P. V., and Chakra, M. (2019). Mineralogy of a New Occurrence of Lamprophyre Dyke from the Saurashtra Peninsula of Gujarat, Northwest Deccan Trap, India. *Journal of the Geological Society of India*, 93:629–637. https://doi.org/10.1007/s12594-019-1241-6

Nixon, A. L., Boone, S. C., Gréau, Y., Kohlmann, F., Theile, M., Noble, W., Prent, A., Foden, J., Barnes, S., Wainwright, A. N., Wade, B., Goemann, K., Gilbert, S., Evans, N. J., Dalton, H., Ware, B., and McInnes, B. I. (2025). Volcanoes to vugs: Demonstrating a FAIR geochemistry framework with a diverse application of major and trace element data through the AuScope EarthBank platform. *Chemical Geology*, 696. https://doi.org/10.1016/j.chemgeo.2025.123092

Pearson, J. M. and Taylor, W. R. (1996). Mineralogy and geochemistry of fenitized alkaline ultrabasic sills of the Gifford Creek Complex, Gascoyne Province, Western Australia. *The Canadian Mineralogist*, 34:201–219.

Pirajno, F. (2004). Metallogeny in the Capricorn Orogen, Western Australia, the result of multiple ore-forming processes. *Precambrian Research*, 128:411–439.

Sheppard, S., Rasmussen, B., Muhling, J. R., Farrell, T. R., and Fletcher, I. R. (2007). Grenvillian-aged orogenesis in the Palaeoproterozoic Gascoyne Complex, Western Australia: 1030–950 Ma reworking of the Proterozoic Capricorn Orogen. *Journal of Metamorphic Geology*, 25:477–494. https://doi.org/10.1111/j.1525-1314.2007.00708.x

Singer, D. A. and Kouda, R. (2001). Some Simple Guides to Finding Useful Information in Exploration Geochemical Data. *Natural Resources Research*, 10.

Slezak, P., Spandler, C., Border, A., and Whittock, K. (2021). Geology and ore genesis of the carbonatite-associated Yangibana REE district, Gascoyne Province, Western Australia. *Mineralium Deposita*, 56:1007–1026. https://doi.org/10.1007/s00126-020-01026-z

Taylor, S. and McLennan, S. (1985). Front cover image for The continental crust, its composition and evolution: an examination of the geochemical record preserved in sedimentary rocks. Blackwell Scientific, Oxford, 312.

Valdiya, K. S. (2015). The Making of India Geodynamic Evolution. Springer, 2 edition. https://doi.org/10.1007/978-3-319-25029-8

Walker, A. T., McInnes, B. I., de Caritat, P., and Bastrakov, E. (2024). Heavy mineral exploration on the continental scale. *EXPLORE (Newsletter for the Association of Applied Geochemists)*, pages 1–13. https://doi.org/10.70499/vwri6466

Wilkinson, M. D. et al. (2016). Comment: The FAIR Guiding Principles for scientific data management and stewardship. *Scientific Data*, 3. https://doi.org/10.1038/sdata.2016.18

Wyche, S., Kirkland, C. L., Riganti, A., Pawley, M. J., Belousova, E., and Wingate, M. T. (2012). Isotopic constraints on stratigraphy in the central and eastern Yilgarn Craton, Western Australia. *Australian Journal of Earth Sciences*, 59:657–670. https://doi.org/10.1080/08120099.2012.697677